國 立 交 通 大 學

電機與控制工程學系

碩 士 論 文

具多圈電極之液晶變焦透鏡及發展其成像品質評估方法

Design of a Multi-ring LC Lens and Development of its
Quantitative Focusing Quality Assessment Method

研 究 生：施凱騰

指導教授：趙昌博 教授

中 華 民 國 九 十 七 年 七 月

具多圈電極之液晶變焦透鏡及發展其成像品質評估方法

Design of a Multi-ring LC Lens and Development of its Quantitative

Focusing Quality Assessment Method

研 究 生：施凱騰 　　　　　Student：Kai-Teng Shih

指導教授：趙昌博 　　　　　Advisor：Paul C.-P. Chao

國 立 交 通 大 學

電 機 與 控 制 工 程 學 系

碩 士 論 文

A Thesis

Submitted to Department of Electrical and Control Engineering

College of Electrical Engineering

National Chiao Tung University

in partial Fulfillment of the Requirements

for the Degree of Master

in

Electrical and Control Engineering

July 2008

Hsinchu, Taiwan, Republic of China

中華民國九十七年七月

具多圈電極之液晶變焦透鏡及發展其成像品質評估方法

學生：施凱騰　　　　　　　　　　　　指導教授：趙昌博

國立交通大學 電機與控制工程 學系（研究所）碩士班

摘要

　　本論文完成具多圈電極之液晶變焦透鏡應用於手機相機的設計。以液晶分子在電場作用下的動態理論做為基礎理論設計，並藉由模擬與分析達到電極圈數的最佳化設計。近年來，由於手機相機搭載自動對焦與變焦系統的趨勢更為彰顯，若液晶變焦透鏡能取代傳統手機鏡頭模組中的透鏡，則可使手機相機同時具備自動對焦與變焦系統並且更為輕巧與降低成本。因此，本文首先根據液晶變焦透鏡的變焦效能來計算實際可取代傳統手機鏡頭模組做為自動對焦與變焦系統的程度。相較於一般手機相機，其鏡頭模組特別需要較短的焦距(約8公分)與較大的孔徑(大於3公厘)，然而這也是目前液晶變焦透鏡無法達成的規格。本文為使改善目前液晶變焦透鏡對於手機相機的應用，而建立一套方法可設計具多圈電極之較大孔徑的液晶變焦透鏡。不僅如此，本文針對液晶變焦透鏡的成像品質亦發展其評估方法，基於點擴散函數與調制轉換函數的光學理論計算而成。藉此成像品質評估方法對具多圈電極之液晶變焦透鏡的電極寬度與圈數做最佳化設計，以達成所需之成像品質的要求。而在此設計之中，液晶變焦透鏡的電極圈數得首先決定，再依據其所需電壓與透鏡半徑位置的斜率變化比例關係來設計多圈電極寬度。最後本文以三圈電極之液晶變焦透鏡做為最佳化設計結果，依據其電極圈數持續增加至七圈時的成像品質無明顯提升。而此三圈電極之液晶變焦透鏡的成像品質，其調制轉換函數分別在65%與48%時可解析至5 Lp/mm與7 Lp/mm。

關鍵詞：液晶變焦透鏡、多圈電極、手機相機、成像品質

Design of a Multi-ring LC Lens and Development of its Quantitative Focusing Quality Assessment Method

Student：**Kai-Teng Shih**　　　　　　　Advisor：**Prof. Paul C.- P. Chao**

Department of Electrical and Control Engineering

National Chiao Tung University

Abstract

The liquid crystal (LC) lens with multi-ring electrodes for cameras in cell phones is designed in this study based on theoretical analysis, simulations and optimization. As the auto-focusing and zooming systems for cameras in cell phones become popular, the applications of a liquid crystal lens to cameras in cell phones provide the advantages such as compact, lightweight, and inexpensive, by replacing the indispensible moving lenses in the traditional lens module. This study starts with the calculations to show that a substantial size reduction of a lens module can be offered by an insertion of LC lens. As compared to conventional cameras, the lens module in phone cameras particularly requires shorter focal length (around 8cm) and larger aperture (greater than 3 mm). The currently available LC lenses, however, fails to provide both the above capabilities. To remedy the problem, the method to design a large-aperture LC lens with multi-ring electrodes is developed in this study, and a new quality-assessment method is developed to evaluate the designed multi-ring LC lens via point spread function (PSF) and modulation transfer function (MTF). The number and widths of the ring-type electrodes are further optimized to reach certain required levels of PSF and MTF for the LC lens. This is achieved by designating a finite number of ring electrodes first and then assigning the width of each electrode proportional to the slope of the

required applied voltage along the radius of the LC lens. Optimization results show that the three-ring LC lens with ring widths particularly designed reached satisfactory MTF of 65% for 5 and 48% for 7 line pairs per millimeter, which are not increased significantly even with the ring number increased to seven.

誌　　謝

本論文得以撰寫完成，首先感謝指導教授 趙昌博老師兩年來對學生在研究上的指導，並適時提供寶貴的研究經驗，使學生在遭遇瓶頸時能夠順利解決，同時亦使學生在研究上獲得莫大的幫助與鼓勵，在此對老師致以最誠摯的感恩。

此外，由衷感謝 黃乙白老師對於研究上的教導與協助，並不時給予學生關心與鼓勵。感謝 黃乙白老師、林怡欣老師於論文審查時不吝指正本論文的缺失與建議，於此致上由衷的謝意。

在研究所生涯中，首先特別感謝祺緯學長與東穎學長在研究與生活上的關照與指導，以及顯示科技所凌嶢學長的協助與幫忙；感謝同窗永原在最後的時刻給予協助。最後，深深感謝我的親人，使我在研究所生涯中給予最大的支持與鼓勵，僅以此論文獻給你們。

Table of Contents

Figure Captions

Table Titles

1 Introduction

Digital cameras in mobile phones are currently inexpensive with satisfactory image definition as compared to conventional cameras, thus increasing consumer requirements and rapid development of camera phone technology. There are three image functions dominating the performance of a digital phone camera. These functions are implemented by the modules of auto-focusing (AF), zooming and auto-white-balance (AWB) [1-2]. Among them, the auto-focusing and zooming functions are the most fundamental one and gradually regarded indispensable by the consumers purchasing a cell phone [3]. Nowadays, a small-sized optical lens module being magnetically actuated is most widely adopted in cell phones thanks to merits of low cost and fast response. However, the implementation of auto-focusing and zooming are realized by traditional motions of some lenses in the optical lens module, which in results, requires certain thickness of the module, leading to the great difficulty to be implemented in the phone cameras. To remedy the problem, a novel LC lens with multi-ring electrodes are designed and optimized, which replaces the moving lens in the aforementioned optical module, and expected to be implemented into the phone cameras. The newly-designed LC lens would be capable of simultaneously achieve short focal length, varying focal length and maintain satisfactory imaging quality.

Lenses are usually made of optical glass owing to that glass has large refractive index and is transparent. In many applications, variable-focus lenses are usually desired. A traditional variable-focus lens is composed of several pieces of glass lenses, and the focus changing is accomplished by mechanical movement of the individual lenses in it. Like glass material, liquid crystal (LC) materials also have large refractive indexes and are transparent, but their electrical and optical properties are anisotropic, and they are widely used to fabricate electro-optic devices. Many applications of LC to optical devices such as optical waveguides,

optical switches, and light deflection devices have been reported. Therefore the optical lens could be realized by the LC materials, and it was proposed over 20 years ago [4]. Compared with the variable-focus lenses made by glass lenses for cameras in cell phones, the LC lens is compact, lightweight, and inexpensive. The advantage of LC Lens is that one can apply non-uniform electric field distribution between the electrodes to tune the focal length. Since the electric field distribution in the LC is non-uniform, therefore how to design the electrode structures and apply the voltage to form the appropriate electric field distribution are very important tasks to control the focal length.

The LC lens has been published since 1979 by Susumu Sato [4]. Susumu Sato uses a thin layer of LC that one is sandwiched between two glass substrates. The structure could change the focal length by electrically controllable method. According to the method, the optical effective could be the same as the optical element of plano-convex lens or plano-concave lens. Since the LC lens was published in 1979, the research of LC lens was conducted and studied widely, and it was enabled many applications such as focal length controllable, the magnification of image, optical axis tunable etc. The researches of Susumu Sato contain the design of focal length controlled by different structures, the solvent of design issues and the design of optical axis tunable. In 1997, Susumu Sato et al. [5] have present a new method to improve the spherical aberration of LC lens by using nematic liquid crystal and an elliptically-patterned electrode structure to observe its interference patterns by a microscope of charge-coupled device (CCD). In 2002, Susumu Sato et al. [6-7] have propose a LC lens with a simple cell structure which it was prepared using a hole-patterned electrode and an intermediate insulating layer, but the design made it difficult for disclination lines to appear. A LC lens with a spherical electrode was proposed by Susumu Sato et al. in 2002 [8-10]. With the transparent indium tin oxide (ITO) film being coated on the spherical surface of a plano-convex glass lens that was placed on a planar LC cell to make the result as a traditional

glass lens does. As the similar structure of LC lens was also proposed by S.-T. Wu et al. in 2004 [11-12]. A tunable focus with spherical lens or spherical glass shell and inhomogeneous electric field over a homogeneous LC layer to fill polymer in the sag region, the focal length was gradually drawn near from infinity to ~96 cm by increasing the applied voltage. A LC lens of two LC layers was proposed to increase the lens focusing power by Susumu Sato et al. in 2004 [13-14]. Its focusing power is electrically tunable and is much larger than two times that of the single-layer LC lens. A cylindrical lens was proposed using two planar substrates and a homogeneous LC layer by S.-T. Wu et al. in 2004 [15]. Based on this design, it was easy to fabricate a cylindrical lens with large aperture size with the tunable range from infinity to 10 cm and the switching time less than 100 ms attributed to the thin cell gap. An adaptive lens using electrically induced LC/monomer concentration redistribution was proposed by S.-T. Wu et al. in 2006 [16]. Application of the LC/monomer mixture electric field causes the LC molecules to diffuse towards the high field region and the liquid monomer towards the low field region. Compared with a conventional LC lens, the tunable focus lens has advantage in small astigmatism and without light scattering, but its response time was slower. A negative LC lens was realized using a two-voltage-driving system by Susumu Sato et al. in 2005 [17-18]. After the negative LC lens, a LC lens with focal length variable from negative to positive was proposed by Susumu Sato et al. in 2006 [19]. There were three electrodes in the LC cell, and the lens was driven by two voltages that produce a spatially non-uniform and symmetrical electric field in the LC layer. A new method was proposed to drive a LC lens with no defects occurring by Susumu Sato et al. in 2003 [20-23]. A voltage difference remains between the two ends of one of the lens' electrodes for a short time and an in-plane electric field from in the LC to prevent the defect of disclination line. A LC lens with focus movable off as well as along the axis was realized by Susumu Sato et al. in 2003 [24-25]. There were two electrodes in the cell: one with a hole and another with resistance and subelectrodes. The focus was adjusted along the axis by the applied

voltage across the two electrodes, and it was also moved off the axis by the voltage across the subelectrodes. A LC lens with focus movable in the focal plane was proposed by Susumu Sato et al. in 2005 [26]. One electrode with hole in the center was divided into four subelectrodes. By applying different potentials to the subelectrodes, a desired asymmetrical phase transformation is formed and off-axis movement of the focus take place. According to the references, the above-mentioned results of past research may apply to cameras in cell phones with LC lens.

According to the advantages and results of past research, the most worthy application of LC lens is used for the camera lens of cell phone in present. Nowadays, the most popular functions of the camera in cell phone are the auto-focusing (AF) and zooming system. If the LC lens could replace some moving lenses of cameras in cell phones, it would not only to reduce the thickness, weight and cost, but also easily make the camera in cell phones having the AF system and the function of zooming at the same time. The LC lens in this study is designed of non-uniform width multiple rings in order to render the focal length required by general phone camera --- which is about 10cm, and simultaneously fine-tune imaging quality via multiple rings. In the next step, to assess the imaging quality of the LC lens quantitatively, the methods are developed based on point spread function (PSF) and modulation transfer function (MTF). According to the above-mentioned assessment methods, the study is further to optimize the LC lens with multi-ring electrodes in different widths and layers. In this way, the newly-designed LC with multiple-ring electrodes performs better than the traditional hole-type LC lens [6-7] in terms of PSFs and MTFs.

2 A Liquid Crystal Lens Applied to Cell Phones

Nowadays, the most popular functions of the camera in cell phone are the auto-focusing (AF) and zooming system. The implementation of auto-focusing and zooming are realized by traditional motions of some lenses in the optical lens module, which in results, requires certain thickness of the module, leading to the great difficulty to be implemented in the phone cameras. As the requirements, if the LC lens could replace some moving lenses of cameras in cell phones, it would not only to reduce the thickness, weight and cost, but also easily make the camera in cell phones having the AF system and the function of zooming at the same time.

2.1 Function of Auto Focusing

2.1.1 The Traditional Auto Focusing System

The auto-focusing (AF) systems usually rely on one actuator and many groups of lens to achieve correct focus. The traditional AF system is shown in Fig. 1. The operation of AF is realized by adjusting the axial positions of a certain group of lens, X', in order to adjust the focal plane to be located in the image sensor. In Fig. 2, the distance X' is derived as followed, [27]

$$d_{camera} = -X - f_{camera} + f'_{camera} + X',$$ (1)

where d_{camera}, f'_{camera} (f_{camera}), X and X' are the distance of shot, the focal length of camera, the distance of object (general around 50 times the focal length of camera) and the distance of image, respectively. From the Newtonian formula $X' \cdot X = -\left(f'_{camera} \right)^2$, Eq. (1) is reorganized as followed,

$$d_{camera} \cdot X' = \left(f'_{camera} \right)^2 + 2 \cdot f'_{camera} \cdot X' + \left(X' \right)^2,$$ (2)

$$\left(X'\right)^2 + \left(2 \cdot f'_{camera} - d_{camera}\right) \cdot X' + \left(f'_{camera}\right)^2 = 0. \tag{3}$$

Defining the parameter $A = 2 \cdot f'_{camera} - d_{camera}$, Eq. (3) is simplified and calculated as followed,

$$\left(X'\right)^2 + A \cdot X' + \left(f'_{camera}\right)^2 = 0, \tag{4}$$

$$X' = \frac{-A \pm \sqrt{A^2 - 4\left(f'_{camera}\right)^2}}{2}. \tag{5}$$

The lens-group-moving distance X' is the difference between the focal plane with finite distance from object (d_{camera}) and the focal plane with infinite distance from object. As shown in Fig.2, with the finite distance from object, the group of lens moves to the object along the optical axis in distance X', and the image plane is maintained in the fixed location.

2.1.2 The New Auto Focusing System including a Liquid Crystal Lens

The advantage of LC lens is that one would generate non-uniform electric field distribution between the electrodes to tune the focal length. According to the function, the traditional AF system in order to adjust the appropriate focal length, it would have to equip the actuator to drive the group of lens. As the result, the AF system for cameras in cell phones would need more thickness to move the group of lens, resulting in higher cost. Based on the reasons, if the LC lens could replace the whole traditional AF system to adjust the appropriate focal length, the actuator and many groups of lens would be reduced. In other words, the thickness and cost of AF system would be reduced for cameras in cell phones. In Table 1 [28], where are the specifications of two general lenses for cameras in cell phones. By the specifications, the lens-group-moving distance is calculated along the optical axis based on the theory of traditional AF system in Eq. (5), as shown in Table 2. As the results of calculation, if the camera in cell phones with lens 1 needs to shoot the object from 600 to 100mm, the traditional AF system has to need more thickness from 0.013 to 0.08mm to adjust the focal length; if the

camera in cell phones with lens 2 needs to shoot the object from 600 to 100mm, the traditional AF system has to need more thickness from 0.019 to 0.12mm to adjust the focal length. Although the distance of movement is not reduced very much if the LC lens replaces the traditional AF system, the cost of the whole traditional AF system is still reduced due to the fact that the actuator in AF system is not needed and the thickness of cell phone lens would be thinner.

2.2 Function of Zooming

2.2.1 The Traditional Zooming System

A zoom lens has a function of variable focal length. For practical photographic applications the position of the second principle plane of the lens from the film plane also must vary to keep the image on the film. The simplest and traditional zoom lens is composed of a positive and negative singlet lens. The variation in focal length is obtained by adjusting the separation of the lenses, and a sharp focus is maintained by varying the distance of the lenses from the film plane. As shown in Fig. 3 is a traditional zooming system. The focal length of the zoom lens depends on the Gullstrand equation because of the equivalent power of two airspaced lenses varied with their separation $d_{separation}$ as below, [29]

$$F = F_1 + F_2 - d_{separation} \cdot F_1 \cdot F_2, \qquad (6)$$

where F, F_1, F_2 and $d_{separation}$ are the equivalent power, the power of first lens A_1, the power of second lens A_2 and the separate distance from first lens to second lens, respectively. The distance of the lenses from the film plane depend on the variation in back focal length $\overline{A_2 F'}$ with separation $d_{separation}$ is

$$\overline{A_2 F'} = \frac{1 - d_{separation} \cdot F_1}{F}. \tag{7}$$

Equation (7) shows how far the negative lens must be from the film plane. The positive lens must be an additional distance $d_{separation}$ from the film plane as below,

$$\overline{A_1 F'} = d_{separation} + \overline{A_2 F'}, \tag{8}$$

where the distance of $\overline{A_1 F'}$ is called the overall length. The traditional function of zooming corresponds to moving the negative lens to the second focal plane of the positive lens, and into coincidence with the film plane. In Fig. 3, where the results of Eq. (6), Eq. (7) and Eq. (8) as the equivalent focal length is varied from 50 to 25mm in 5mm steps. The movement of the negative lens is linear with respect to focal length. However, the positive lens requires a special cam to position it appropriately. Consequently, the traditional function of zooming works by the varied of the distance $\overline{A_2 F'}$ to determine the separation $d_{separation}$ and the effective focal length of zoom lens when the focal length of positive lens (A_1) and negative lens (A_2) are all fixed.

2.2.2 The New Zooming System including Liquid Crystal Lens

The characteristic of the zooming system is that one could vary the focal length in camera. A traditional zooming system is composed of several pieces of glass lenses, and the focus changing is accomplished by mechanical movement of the individual lenses in it. Therefore, if the camera in cell phones with the traditional function of zooming, the thickness and weight would be increased. In present, cameras in cell phones are required to be more lightweight and compact. As the requests, if the LC lens could replace the traditional function of zooming to vary the focal length, the LC lens will be only to apply the appropriate electric field distribution between the electrodes, and the function of zooming for cameras in cell phones

will be easily to realize without thickness and weight. In this study, the diameter of effective aperture for LC lens is 3mm and the variable range of focal length is from 130 to 550mm by applying the voltage from $50V_{rms}$ to $10V_{rms}$ in our laboratory. Since the focal length of LC lens is too large for the camera lens in cell phone, there has to assemble one general positive or negative lens to reduce it when the LC lens represent a negative or positive lens. In Table 3, where are the specifications of general optical glass lens with diameter 3mm. According to the above-mentioned specifications, the variation in focal length of LC lens is calculated based on the theory of traditional zooming system, and the variation makes the camera in cell phones with the function of zooming. Since the LC lens would represent a positive or negative lens in different states, the different components of its fitting lens would be also altered to result in different variations of focal length.

2.2.2.1 The Zooming System Including Positive Liquid Crystal Lens

A zooming system including a positive LC lens for cameras in cell phones is shown in Fig. 4. In order to reduce the focal length of positive LC lens for cameras in cell phones, the LC lens has to assemble one general negative lens. Since the LC lens is the structure of two parallel ITO electrodes, the general negative lens would be one optical plano-concave lens to fit the LC lens. Therefore, the focal length of positive LC lens ($f_{LC\ Lens}$) and optical plano-concave lens (f_{Lens}) would be reduced ($f_{Reduced\ Lens}$) by the Gullstrand equation. After reducing the focal length of LC lens, the reduced lens is represented by the variable negative singlet lens (A_2). Because of the simplest zooming system is composed of a positive and negative singlet lens, the zooming system including positive LC lens is completed by adding one general positive singlet lens (A_1). The variable focal length of LC lens from $f_{LC\ Lens}^{1x}$ to $f_{LC\ Lens}^{2x}$ is determined by the variable effective focal length of zooming system from f_{EFL}^{1x} to f_{EFL}^{2x} based on the Gullstrand equation. The relative formulas for zooming system including positive LC lens are

derived as followed where the reduced lens in it is equivalent a variable negative singlet lens. According to the design of zooming system including positive LC lens, the focal length of reduced lens that is varied before ($f_{Reduced\ Lens}^{1x}$) has to calculate in priori as below,

$$F_{Reduced\ Lens}^{1x} = F_{LC\ Lens}^{1x} + F_{Lens} - d_1 \cdot F_{LC\ Lens}^{1x} \cdot F_{Lens}, \quad (9)$$

where $F_{Reduced\ Lens}^{1x}$, $F_{LC\ Lens}^{1x}$ and F_{Lens} are the power of reduced lens that the focal length of positive LC lens is varied before, the power of positive LC lens that the focal length is varied before and the power of optical plano-concave lens, respectively. In Eq. (9), the distance d_1 is separated from LC lens to optical plano-concave lens and it is designed as two lens close together ($d_1 = 0$). After the calculation of $f_{Reduced\ Lens}^{1x}$, the focal length of general positive singlet lens (f_1) is calculated with that the effective focal length of zooming system is f_{EFL}^{1x} as below,

$$F_{EFL}^{1x} = F_1 + F_{Reduced\ Lens}^{1x} - d_2 \cdot F_1 \cdot F_{Reduced\ Lens}^{1x}, \quad (10)$$

where F_{EFL}^{1x} and F_1 are the power of zoom lens that the effective focal length is varied before, the power of general positive singlet lens, respectively. In Eq. (10), the distance d_2 is separated from reduced lens to general positive singlet lens and it is designed as two lens close together ($d_2 = 0$). As the conditions in Eq. (10) that the focal length of general positive singlet lens is fixed and the focal length of reduced lens is variable, the focal length of positive LC lens is varied with the effective focal length of zooming system varied from f_{EFL}^{1x} to f_{EFL}^{2x}. Based on the conditions, the varied focal length of reduced lens ($f_{Reduced\ Lens}^{2x}$) is calculated as below,
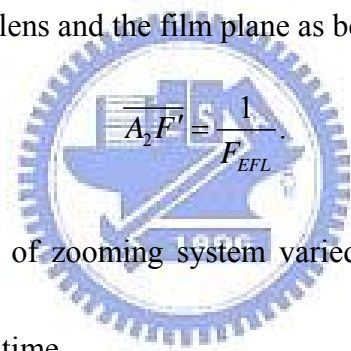
$$F_{EFL}^{2x} = F_1 + F_{Reduced\ Lens}^{2x}, \quad (11)$$

where F_{EFL}^{2x} and $F_{Reduced\ Lens}^{2x}$ are the power of zoom lens that the effective focal length is varied and the power of reduced lens that the focal length of positive LC lens is varied, respectively. Therefore, the varied focal length of the positive LC lens ($f_{LC\ Lens}^{2x}$) is calculated by the varied focal length of the reduced lens and the focal length of optical plano-concave lens as below,

$$F_{Reduced\ Lens}^{2x} = F_{LC\ Lens}^{2x} + F_{Lens}, \qquad (12)$$

where $F_{LC\ Lens}^{2x}$ is the power of positive LC lens that the focal length is varied. Consequently, the zooming system including positive LC lens works by the varied distance $\overline{A_2 F'}$ that the distance is between the reduced lens and the film plane as below,

$$\overline{A_2 F'} = \frac{1}{F_{EFL}}. \qquad (13)$$

With the effective focal length of zooming system varied from f_{EFL}^{1x} to f_{EFL}^{2x}, the distance $\overline{A_2 F'}$ is also varied at the same time.

As the above-mentioned deriving, the varied effective focal length of zooming system from f_{EFL}^{1x} to f_{EFL}^{2x} has to work by the focal length of positive LC lens varied from $f_{LC\ Lens}^{1x}$ to $f_{LC\ Lens}^{2x}$. According to the design of zooming system including positive LC lens, the movement $\overline{A_2 F'}$ and the separation $d_{separation}$ for the traditional zooming system are reduced for cameras in cell phones. Based on the above-mentioned design, the results of zooming system including positive LC lens for cameras in cell phones with the function of zooming are calculated. The specifications for calculating and its results are shown in Table 4 and Fig. 5, where Form f_{EFL}^{1x} to f_{EFL}^{2x}, f_{Lens}, f_1 and From $f_{LC\ Lens}^{1x}$ to $f_{LC\ Lens}^{2x}$ are the variation in effective focal

length of zoom lens, the focal length of optical plano-concave lens, the focal length of general

positive singlet lens and the variation in focal length of positive LC lens, respectively. Use the

same specifications of reduced lens that one represents a variable negative singlet lens to

replace the negative singlet lens in traditional zooming system. In other words, the focal length

f_2 is replaced by the focal length $f_{Reduced\ Lens}$. By the replaced and the same specifications of

Form f_{EFL}^{1x} to f_{EFL}^{2x} and f_1 in Table 4, the movement saved by LC lens and the separation

$d_{separation}$ for traditional zooming system are calculated, as shown in Table 5. Compared with

the results of calculation in Table 4 and Table 5, the zooming system including positive LC lens

is proved more lightweight and compact than traditional one applied to cameras in cell phones

in the same zooming range from f_{EFL}^{1x} to f_{EFL}^{2x}.

2.2.2.2 The Zooming System Including Negative Liquid Crystal Lens

A zooming system including a negative LC lens for cameras in cell phones is shown in Fig. 6.

In order to reduce the focal length of negative LC lens for cameras in cell phones, the LC lens

has to assemble one general positive lens. Since the LC lens is the structure of two parallel ITO

electrodes, the general positive lens would be one optical plano-convex lens to fit the LC lens.

Therefore, the focal length of negative LC lens ($f_{LC\ Lens}$) and optical plano-convex lens (f_{Lens})

would be reduced ($f_{Reduced\ Lens}$) by the Gullstrand equation. After reducing the focal length of

LC lens, the reduced lens is represented the variable positive singlet lens (A_1). By the similar

way to vary the focal length of LC lens in section 2.2.2.1, the zooming system including

negative LC lens is completed by adding one general negative singlet lens (A_2). The relative

formulas for zooming system including negative LC lens are derived as followed where the

reduced lens in it is equivalent a variable positive singlet lens. According to the design of

zooming system including negative LC lens, the focal length of reduced lens that is varied

before ($f^{1x}_{Reduced\ Lens}$) also has to calculate in priori by the similar formula in Eq. (9), where

$F^{1x}_{Reduced\ Lens}$, $F^{1x}_{LC\ Lens}$ and F_{Lens} are the power of reduced lens that the focal length of negative

LC lens is varied before, the power of negative LC lens that the focal length is varied before

and the power of optical plano-convex lens, respectively. In Eq. (9), d_1 is the distance

separate from LC lens to optical plano-convex lens is also designed as two lens close together

($d_1 = 0$). After the calculation of $f^{1x}_{Reduced\ Lens}$, the focal length of general negative singlet lens

(f_2) is calculated with that the effective focal length of zooming system is f^{1x}_{EFL} as below,

$$F^{1x}_{EFL} = F^{1x}_{Reduced\ Lens} + F_2 - d_2 \cdot F^{1x}_{Reduced\ Lens} \cdot F_2, \tag{14}$$

where F_2 is the power of general negative singlet lens, and the distance d_2 separated from

reduced lens to general negative singlet lens is also designed as two lens close together ($d_2 = 0$)

in Eq. (14). As the conditions in Eq. (14) that the focal length of general negative singlet lens is

fixed and the focal length of reduced lens is variable, the focal length of negative LC lens is

varied with the effective focal length of zooming system varied from f^{1x}_{EFL} to f^{2x}_{EFL}. Based on

the conditions, the varied focal length of the reduced lens ($f^{2x}_{Reduced\ Lens}$) is calculated as below,

$$F^{2x}_{EFL} = F^{2x}_{Reduced\ Lens} + F_2, \tag{15}$$

where $F^{2x}_{Reduced\ Lens}$ is the power of reduced lens that the focal length of negative LC lens is

varied. Therefore, the varied focal length of the negative LC lens ($f^{2x}_{LC\ Lens}$) is calculated by the

varied focal length of the reduced lens and the focal length of optical plano-convex lens, as the

similar formula in Eq. (12), where $F^{2x}_{LC\ Lens}$ is the power of negative LC lens that the focal

length is varied. Consequently, the zooming system including negative LC lens works by the

varied distance $\overline{A_2F'}$ that the distance is between the reduced lens and the film plane as also

shown in Eq. (13). With the effective focal length of zooming system varied from f_{EFL}^{1x} to

f_{EFL}^{2x}, the distance $\overline{A_2F'}$ is also varied at the same time.

As the above-mentioned deriving, the varied effective focal length of zooming system from

f_{EFL}^{1x} to f_{EFL}^{2x} has to work by the focal length of positive LC lens varied from $f_{LC\,Lens}^{1x}$ to

$f_{LC\,Lens}^{2x}$. According to the design of zooming system including negative LC lens, the movement

$\overline{A_2F'}$ and the separation $d_{separation}$ for the traditional zooming system are reduced for cameras

in cell phones. Based on the above-mentioned design, the results of zooming system including

negative LC lens for cameras in cell phones with the function of zooming are calculated. The

specifications for calculating and its results are shown in Table 6 and Fig. 7, where

Form f_{EFL}^{1x} to f_{EFL}^{2x}, f_{Lens}, f_2 and From $f_{LC\,Lens}^{1x}$ to $f_{LC\,Lens}^{2x}$ are the variation in effective focal

length of zoom lens, the focal length of optical plano-convex lens, the focal length of general

negative singlet lens and the variation in focal length of negative LC lens, respectively. Use the

same specifications of reduced lens that one represents a variable positive singlet lens to

replace the positive singlet lens in traditional zooming system. In other words, the focal length

f_1 is replaced by the focal length $f_{Reduced\,Lens}$. By the replaced and the same specifications of

Form f_{EFL}^{1x} to f_{EFL}^{2x} and f_2 in Table 6, the movement saved by LC lens and the separation

$d_{separation}$ for traditional zooming system are calculated, as shown in Table 7. Compared with

the results of calculation in Table 6 and Table 7, the zooming system including negative LC

lens is also proved more lightweight and compact than traditional one applied to cameras in

cell phones in the same zooming range from f_{EFL}^{1x} to f_{EFL}^{2x}.

3. Designing the Liquid Crystal Lens with Multi-ring Electrodes

As compared to conventional cameras, the lens module in phone cameras particularly requires shorter focal length and larger aperture. The currently available LC lenses, however, fails to provide both the above capabilities. To remedy the problem, the method to design non-uniform width multiple rings in order to render the focal length and the aperture required by general phone camera is developed.

3.1 Theory of Gradient Index Lens

An ordinary homogeneous lens has two physical features that contribute to the manner in which it reconfigures a wavefront: the difference between its index of refraction and that of the surrounding medium, and the curvature of its interfaces. As the known formula, $v = c/n$, where c, n and v are the velocity in vacuum, index of refraction and the velocity in medium, respectively. As the light propagating through an inhomogeneous medium, wavefronts essentially slow down in optically dense regions and speed up in less dense region. In principle, the lens from some inhomogeneous material is such as the gradient in the index of refraction; such the device is called the GRIN Lens (GRadient INdex Lens) [30]. Consider the device as shown in Fig. 8, for simplicity, assume $f > r$. The GRIN Lens is a flat disk of glass that has been treated so that the lens has an index $n(r)$ that drops off radially in some as yet undetermined fashion from a maximum value of $n(r)_{max}$ on the optical axis. A ray that traverses the lens on the optical axis passes along an optical path length (OPL) of $(OPL)_{axis} = n(r)_{max} \cdot d$, whereas for a ray traversing at a height r, overlooking the slight bending of its path, $(OPL)_r \approx n(r) \cdot d$. Since a planer wavefront must bend into a spherical wavefront, the OPLs from one to the other, along any route must be equal as followed,

$$(\text{OPL})_r + \overline{AB} \cong (\text{OPL})_{axis}, \tag{16}$$

and

$$n(r) \cdot d + \overline{AB} \cong n(r)_{max} \cdot d. \tag{17}$$

But $\overline{AF} \approx \sqrt{r^2 + f^2}$; moreover, $\overline{AB} = \overline{AF} - f$ and so

$$n(r) = n(r)_{max} - \frac{\sqrt{r^2 + f^2} - f}{d}. \tag{18}$$

According to the square roots that via the Binomial Theorem ($\sqrt{r^2 + f^2} \approx f\left[1 + \frac{1}{2}\left(\frac{r}{f}\right)^2\right]$),

Eq. (18) is simplified as

$$n(r) = n(r)_{max} - \frac{r^2}{2fd}. \tag{19}$$

As the result, if the index of refraction drops off parabolically from its high along the central axis, the GRIN plate would focus a collimated beam at point F and serve as a positive lens. Moreover, Eq. (20) is simplified from Eq. (19) as below,

$$f = \frac{r^2}{2d \cdot \left[n(r)_{max} - n(r)\right]} = \frac{r^2}{2d \cdot \Delta n(r)}. \tag{20}$$

From Eq. (20), the focal length is varied by the thickness of the lens (d) and the difference in index of refraction ($\Delta n(r)$) or the radius of lens (r).

3.2 Developing the Design for the Liquid Crystal Lens with Multi-ring Electrodes

In order to render better performance from the LC lens, designs of the electrodes and relative voltage to form the appropriate distribution of non-uniform electric field are very important tasks. The effective index distribution of refraction of LC lens is yielded with the non-uniform electric field by the properties of dielectric behavior. Effects due to conductivity of the LC have been neglected. In this study, the nematic liquid crystal is used to be the LC material of LC lens with multi-ring electrodes. By the orientation of nematic liquid crystals in an electric field between two electrode plates as shown in Fig. 9, the tilting angle of LC molecules in LC layer of the LC lens is calculated by Eq. (21) and Eq. (22) as below, [31]

$$\frac{V}{V_o} = \frac{2}{\pi} \int_0^{\phi_m} \frac{\sqrt{(1+\kappa \sin^2 \phi)(1+\gamma \sin^2 \phi_m)}}{\sqrt{(1+\kappa \sin^2 \phi)(\sin^2 \phi_m - \sin^2 \phi)}} d\phi, \tag{21}$$

and

$$z' = \frac{d}{2} \cdot \frac{\int_0^{\phi} \sqrt{\frac{(1+\kappa \sin^2 \phi)(1+\gamma \sin^2 \phi_m)}{\sin^2 \phi_m - \sin^2 \phi}} d\phi}{\int_0^{\phi_m} \sqrt{\frac{(1+\kappa \sin^2 \phi)(1+\gamma \sin^2 \phi_m)}{\sin^2 \phi_m - \sin^2 \phi}} d\phi}, \tag{22}$$

where V, V_o, ϕ, ϕ_m, z' and d are the applied voltage, the threshold voltage, the tilting angle of LC molecule, the maximum tilting angle at the center of LC layer, the coordinate in the direction of optical axis and the thickness of LC layer, respectively. The parameters of V_o, κ and γ are represented as Eq. (23), Eq. (24) and Eq. (25),

$$V_o = \pi \left(\frac{k_{11}}{\varepsilon_0 (\varepsilon_\parallel - \varepsilon_\perp)} \right)^{1/2}, \tag{23}$$

$$\gamma = \frac{\varepsilon_\parallel - \varepsilon_\perp}{\varepsilon_\perp}, \tag{24}$$

and

$$\kappa = \frac{k_{33} - k_{11}}{k_{11}}, \qquad (25)$$

where $\varepsilon_\parallel$, $\varepsilon_\perp$, K_{11} and K_{33} are the relative dielectric permittivity parallel to the director of

molecules, the relative dielectric permittivity perpendicular to the director of molecules, the

elastic curvature constants of splay and the elastic curvature constants of bend, respectively.

The maximum tilting angle ϕ_m is determined corresponding to an applied voltage V from

Eq. (21). The tilting angle ϕ is a function of coordinate z' from Eq. (22), $\phi(z')$ assuming

a maximum tilting angle value ϕ_m at $z' = d/2$ and being 0 at the boundaries ($z' = 0$). In this

study, the relative parameters of nematic LC are shown in Table 8. With the parameters and

assuming the range of ϕ_m from 0° to 90°, the relations of function $V(\phi_m)$ form Eq. (21)

and $\phi(z')$ from Eq. (22) by given the range of ϕ_m are calculated as shown in Fig. 10 and

Fig. 11. The calculations assume that the orientation of nematic liquid crystal in the distance

from 0 to $d/2$ and from d to $d/2$ of the LC layer is symmetric. According to the

assumption, the calculating results only present the range from 0 to $d/2$ of the LC layer to

analyze. In Fig. 10, the maximum tilting angle ϕ_m is determined by its corresponding applied

voltage. In Fig. 11, each curve of function $\phi(z')$ is represented its corresponding maximum

tilting angle ϕ_m from 0° to 90°, and the curve is also shown its distribution of tilting angle

ϕ at any position in the coordinate of optical axis (from 0 to $d/2$). According to the

calculating result from Eq. (22), the index refraction is calculated by each tilting angle ϕ

which results from each curve of function $\phi(z')$ as below, [32]

$$n_{eff}(\phi) = \frac{n_o n_e}{\sqrt{n_e^2 \sin^2\phi + n_o^2 \cos^2\phi}}, \qquad (26)$$

where n_e and n_o are the extraordinary and the ordinary index refraction of nematic liquid

crystal in this study, respectively. As the results of calculation from each tilting angle ϕ with the parameters of n_e and n_o, the effective index of refraction ($n_{eff}(r)$) is calculated by the method of integration. According to the calculation by the method of integration in Eq. (26), the effective index of refraction $n_{eff}(r)$ from each maximum tilting angle ϕ_m (from 0° to 90°) with its distribution of tilting angle ϕ is calculated, as shown in Fig. 12. Since the effective index distribution of refraction ($n_{eff}(r)$) at the center of the LC lens with structure of hole-type in our laboratory is not similar to the index distribution of GRIN lens, the improvement of the design for the LC lens with multi-ring electrodes is that the effective index distribution of refraction is as far as possible to design as GRIN lens. The effective focal length of the LC lens with structure of hole-type in our laboratory is about 112mm by given the voltage $50V_{rms}$ which the diameter of effective aperture and the length of square shape are 3mm and 20mm respectively. In order to improve the LC lens with structure of hole-type in our laboratory, the LC lens with multi-ring electrodes is also designed with the same specifications of focal length and diameter of effective aperture. Based on the principle of the design for the LC lens with multi-ring electrodes, the above-mentioned calculations for effective index of refraction $n_{eff}(r)$ is used to represent the effective index distribution of refraction that the distribution is according to the maximum tilting angle ϕ_m from center to the radius of effective aperture (from 0° to 90°) as shown in Fig. 13. With the effective index distribution of refraction $n_{eff}(r)$ and given the required focal length, the radius of effective aperture of the LC lens with multi-ring electrodes is determined by the theory of GRIN lens as below,

$$f = \frac{r^2}{2 \cdot d \cdot \Delta n_{eff}(r)} = \frac{r^2}{2 \cdot [\int_0^d (n_{eff}(0,z'))dz' - \int_0^d (n_{eff}(r,z'))dz']}, \qquad (27)$$

where r and d are the variable radius of LC lens and the thickness of LC layer, respectively. The effective index distribution of refraction $n_{eff}(r)$ is represented that each effective index of refraction $n_{eff}(r)$ is distributed at the radius of effective aperture from $-r$ to r of the LC lens with multi-ring electrodes. For the design of the distribution of maximum tilting angle ϕ_m is from 0° to 90° at the radius of effective aperture from center to r and from 90° to 0° at the radius of effective aperture from $-r$ to center. In Eq. (27), the difference in effective index distribution of refraction ($\Delta n_{eff}(r)$) of the LC lens with multi-ring electrodes means that the difference between the integration of the effective index of refraction $n_{eff}(r)$ at center and at the radius of effective aperture r. According to Eq. (27), the effective index distribution of refraction $n_{eff}(r)$ would only represented a function of the radius r as given the required focal length f of the LC lens with multi-ring electrodes. Since the design of the LC Lens with multi-ring electrodes assumes circularly symmetry, the effective index distribution of refraction $n_{eff}(r)$ from the radius of effective aperture $-r$ to 0 and from the radius of effective aperture 0 to r is also symmetric for perfect design. With the assuming of symmetry, the results of calculation only present the radius of effective aperture from 0 to r of the LC lens with multi-ring electrodes to analyze. As the above-mentioned calculations for effective index distribution of refraction $n_{eff}(r)$ and the symmetrical assumption, the effective index distribution of refraction $n_{eff}(r)$ of the LC lens with multi-ring electrodes related to its radius of effective aperture r is calculated by Eq. (27) as given the focal length $f = 112mm$, the calculating results as shown in Fig. 14. By the effective index distribution of refraction $n_{eff}(r)$ of the LC lens with multi-ring electrodes, the phase retardation ($\delta(r)$) is calculated as below,

$$\delta(r) = \frac{2\pi}{\lambda} \cdot \Delta n_{eff}(r) \cdot d = \frac{2\pi}{\lambda} \cdot \left[\int_0^d (n_{eff}(r,z'))dz' - \left(\int_0^d (n_{eff}(r,z'))dz' \right)_{\min} \right]. \qquad (28)$$

As the calculating results in Fig. 14, the phase retardation δ of the LC lens with multi-ring electrodes is calculated without the multiplication of $2\pi/\lambda$ by Eq. (28), as shown in Fig. 15. Based on the calculating results of the effective index distribution of refraction $n_{eff}(r)$ and the phase retardation $\delta(r)$ for the LC lens with multi-ring electrodes as shown in Fig. 12 and Fig. 14 respectively, each maximum tilting angle ϕ_m is corresponding to its effective index of refraction $n_{eff}(r)$, and the effective index of refraction $n_{eff}(r)$ is corresponding to its radius of effective aperture r. According to the relations of calculating result, the distribution of maximum tilting angle ϕ_m from 0° to 90° is related to the radius of effective aperture r, as the function of $\phi_m(r)$ shown in Fig. 16. Since the effective index distribution of refraction $n_{eff}(r)$ of the LC lens with multi-ring electrodes is not distinct variation from center to $r = 0.2 \text{mm}$ in Fig. 14, the maximum tilting angle ϕ_m at the radius of effective aperture from center to $r = 0.2 \text{mm}$ is designed as 0°, and it also makes sure that the effective index of refraction $n_{eff}(r)$ at center is the maximum. According to the results of function $V(\phi_m)$ form Eq. (21) as shown in Fig. 10 and the above-mentioned results of function $\phi_m(r)$ as shown in Fig. 16 respectively, the applied voltage V is related to the radius of effective aperture r, as the function of $V(r)$ shown in Fig. 17. Finally the design principle of the LC lens with multi-ring electrodes is based on the slope of $V(r)$ (denoted by dV/dr) to determine each width of ring electrodes in the effective aperture, as shown in Fig. 18.

According to the calculating results in Fig. 18, the numerical values of slope dV/dr are shown in Table 9 to be the reference for the design of the width of multi-ring electrodes,

where the No. of position, the position of radius, the width of electrode, the range of slope

(dV/dr) and the difference in range of slope ($\Delta(dV/dr)$) are shown in it respectively.

According to the numerical values in Table 9, the numerical values of $\Delta(dV/dr)$ with its

corresponding position of radius are separated into some regularity in the varied range of

slope. As the results in Table 9 obvious that the slope range considered are separated into

some ranges with the corresponding position of radius such as the range from 0.25 to 0.3,

from 0.2 to 0.25, from 0.15 to 0.2, from 0.1 to 0.15, from 0 to 0.05, from 0.01 to 0.05, from 0

to 0.01, from 0.01 to 0.02, from 0.02 to 0.03 and from 0.01 to 0.02, respectively. According to

the separated ranges, some numerical values of $\Delta(dV/dr)$ with the corresponding position

of radius are distributed to its slope range considered. With the redistributions by the slope

range considered, the numerical values of the position of radius and the width of electrode in

Table 9 are separated into 12 groups as shown in Table 10. As the results in Table 10, the

numerical results of the difference in varied range of slope are calculated, and it is used to

design the width of electrodes for LC lens with multi-ring electrodes. Moreover, the design

principle of each width of electrodes is according to the same numerical value of difference in

varied range of slope designed as one electrode, and it is still keeping the theorem that the

width of electrode is increased with the decrease of difference in range of slope $\Delta(dV/dr)$.

Since the diameter of effective aperture and the length of square shape have been determined

in this study, the width of side electrode or the hole-type electrode of LC lens with multi-ring

electrodes also has determined that one is 8500μm. Since the maximum tilting angle ϕ_m at

the radius of effective aperture from center to $r = 0.2\text{mm}$ has been designed as $0°$, the

width of central electrode or the first ring of LC lens with multi-ring electrodes also has

determined that one is 0.2mm by given $0V_{\text{rms}}$. Based on the above design of width for the

hole-type and the first ring electrodes, the LC lens with multi-ring electrodes has been owned

first ring initially. As the above-mentioned designs, the LC lens with multi-ring electrodes in this study would like to design the number of ring electrodes from two to seven rings, as shown in Table 11-16, where are shown the widths of each ring with its corresponding position of radius and its corresponding range of group with the slope range considered respectively. As the results of design, the applied voltage V to each electrode of the LC lens with multi-ring electrodes is corresponding to its position of radius by the function of $V(r)$, as shown in Fig. 17. At the moment of applied voltage $V(r)$, the results are given between two electrode plates with the thickness d of LC layer, and the electric field $E_{LC}(r)$ between two electrode plates is yielded in the LC layer.

Since the multi-ring electrodes of LC lens are designed in the same layer, the ring electrodes would not be complete in order to put the conducting wire in the same layer. As the design of LC lens with multi-ring electrodes, the defect of performance is yielded cause of that the ring electrodes are not complete to affect the distribution of electric field. In order to improve the defect of performance, the multi-ring electrodes of LC lens are designed in different layers in this study, as shown in Fig. 19, where the LC lens with the number of ring electrodes from two to seven rings are shown respectively. The widths of ring electrode for each LC lens with the number of ring electrodes from two to seven rings are shown from Table 11 to Table 16, respectively. In order to show the thicknesses and materials of the LC lens with multi-ring electrodes in different layers simply in Fig. 19, the LC lens with three-ring electrodes in different layers is represented to illustrate the relative thicknesses and materials, as shown in Fig. 20, where the thicknesses and materials are also shown in Table 8. In the processes of fabrication for the LC lens with multi-ring electrodes in different layers, in order to show it simply, the LC lens with three-ring electrodes in different layers is also represented to illustrate the relative size of the conducting wire, the conducting plate and the

photo mask, as shown in Fig. 21, where the upper view of the LC lens with three-ring electrodes in different layers is shown in Fig. 21(a). The hole-type electrode, the first ring electrode, the second ring electrode and the third ring electrode of the LC lens with three-ring electrodes in different layers are shown in Fig. 21(b), Fig. 21 (c), Fig. 21(d) and Fig. 21(e), respectively. As shown in Fig. 21, the each width of conducting wire, the each long side of conducting plate and the each short side of conducting plate are 40μm, 5mm and 2mm, respectively, and all materials are also ITO. In the processes of fabrication for the LC lens with multi-ring electrodes in different layers, the photo mask in Fig. 21(f) is used to expose the conducting plates where the size is the same with conducting plates. By the simply way to explain the method how to expose the conducting plates, the LC lens with three-ring electrodes in different layers is used to represent the process. According to the structure of LC lens with three-ring electrodes in different layers in Fig. 21(a) and by the photo mask in Fig. 21(f), since the four conducting plates are designed at the side of LC lens respectively, in order to expose the four conducting plates that the time for etching by the photo mask are different according to the distance of thickness from the most upper isolation layer to its conducting plate.

As the design of structure for LC lens with multi-ring electrodes in different layers, the thickness between two electrode plates that is the distance from bottom to top electrode are altered with the top ring electrode in different layers. By the alternation of thickness between two electrode plates, the numerical values of applied voltage $V_{Single\text{-}layer}$ from the function of $V(r)$ also have to modify at the same time. According to the numerical values of applied voltage $V_{Single\text{-}layer}$, the electric field as the function of r is calculated,

$$E_{LC}(r) = \frac{V_{Single\text{-}layer}(r)}{d}. \tag{29}$$

The electric field ($E_{LC}(r)$) between two electrode plates is calculated with the applied voltage $V(r)$ and the thickness d of LC layer by Eq. (29). According to the function of $V(r)$, the electric field $E_{LC}(r)$ between the thickness d of LC layer is also different from the position of radius r. Since ring electrodes are designed in different layers of LC lens, the thickness d between two electrode plates is not only the thickness of LC layer. In other words, the thickness d of LC layer is added the thickness of glass and isolation layer that is used the thickness $d_{multi\text{-}layer}$ to represent. In order to maintain the distribution of electric field $E_{LC}(r)$ which is different from the position of radius r, the applied voltage is modified by the changed thickness $d_{multi\text{-}layer}$ that is used the voltage $V_{multi\text{-}layer}$ to represent as below,

$$V_{multi\text{-}layer}(r) = E_{LC}(r) \cdot d_{multi\text{-}layer}. \tag{30}$$

The calculating results by Eq. (30) for each LC lens with the number of ring electrodes from two to seven rings are shown in Table 17-22, respectively. Consequently, any size of aperture for the LC lens with multi-ring electrodes in different layers is designed based on the method of above-mentioned design rules.

According to the results of the design for the LC lens with the number of ring electrodes from two to seven rings in different layers, the width of each ring electrode and its applied voltage $V_{multi\text{-}layer}$ for simulation are reorganized and determined, as shown in Table 23-28 respectively. The determinative step of applied voltage $V_{multi\text{-}layer}$ for each ring electrode is that the hole-type electrode has to determine in priori and others are opened at the moment to make sure the image in the focal plane is near to be distinct. After the determinative applied voltage $V_{multi\text{-}layer}$ of the hole-type electrode, other ring electrodes of the LC lens with

multi-ring electrodes in different layers is given the applied voltage $V_{multi\text{-}layer}$ to improve the

defects of the LC lens only with single-hole electrode. Based on the reason, the first ring

electrode is always given $0V_{rms}$ and others are given the minimum in the range of applied

voltage $V_{multi\text{-}layer}$ initially. According to the performance of the LC lens with multi-ring

electrodes in different layers by given the initial applied voltage $V_{multi\text{-}layer}$, then each ring

electrode is used to tune the performance to reach the best by altering the applied voltage

$V_{multi\text{-}layer}$, besides the hole-type electrode and the first ring electrode. According to the

specifications in Table 8, the simulation for tilt angles θ of the dynamic LC molecules in the

LC lens with multi-ring electrodes in different layers are obtained by using the software

package 2dimMOS^{TM}. The electrostatic and liquid crystal orientation problems are coupled

together and they have been addressed by using the commercially available software package

2dimMOS^{TM} from Autronic-Melchers, as shown in Fig. 22. The tilt angles (θ) which are

between optical axis and liquid crystal molecules of dynamic liquid crystal molecules in the

LC lens are obtained by using the software of 2dimMOS^{TM} to simulate, as shown in Fig. 23.

According to the simulation of the tilt angle θ, the effective index of refraction is greatly

simplify investigation of anisotropic media by treating the propagation of light with an angle

θ to $\bar{n}$ with a refractive index $n_{eff}(\theta)$ in Eq. (31), as shown in Fig. 24, [32]

$$n_{eff}(\theta) = \frac{n_o n_e}{\sqrt{n_e^2 \cos^2\theta + n_o^2 \sin^2\theta}}. \tag{31}$$

Since the tilt angle θ of the liquid crystal molecules in the LC layer are not uniform with

that the electrodes are given by any voltage, the tilt angle θ is a function of coordinate z'

and the maximum tilting angle value θ_m of $\theta(z')$ is at $z' = d/2$, where d is the

thickness of LC layer. According to the calculation by the method of integration in Eq. (31),

the effective index of refraction $n_{eff}(r)$ from the maximum tilting angle θ_m with its

distribution of tilting angle θ is calculated. As the calculating results by integration in Eq.

(31), the effective index distribution of refraction is represented the effective index of

refraction $n_{eff}(r)$ at any position of the radius r of LC lens, as shown in Fig. 25. By the

simulation, the effective index distribution of refractive $n_{eff}(r)$ of the LC lens with the

number of ring electrodes from two to seven rings in different layers is calculated. Compared

with the index distribution of GRIN lens which the focal length is also 112mm (Ideal case)

and the effective index distribution of refractive $n_{eff}(r)$ of LC lens is illustrated in Fig. 26.

4. Developing the Quantitative Assessment Method for Imaging Quality

Since the point spread function (PSF) and modulation transfer function (MTF) are generally used to quantitate imaging quality assessment of optical lenses, the quantitative imaging quality assessment of a LC lens also based on PSF and MTF are developed.

4.1 Point Spread Function of the Liquid Crystal Lens

The point spread function (PSF) is a quantitative criterion to assess the focusing capability for optical lens. Based on the quantitative criterion, the focusing capability of LC lens also uses PSF to assess it. Since the profile of PSF is related to its variation of phase, the phase retardation of LC lens is calculated in priori. The phase retardation $\delta(x, y)$ is

$$\delta(x, y) = \frac{2\pi}{\lambda} \cdot \Delta n(x, y) \cdot d,$$
(32)

where λ, $\Delta n(x, y)$ and d are the wave length, the difference of refractive index and the thickness of liquid crystal layer, respectively. The transmittance of the LC lens as a complex function $t(x, y)$ is

$$t(x, y) = \frac{U_2(x, y)}{U_1(x, y)} = P(x, y) \exp\left[-i\delta(x, y)\right],$$
(33)

where the $U_1(x, y)$ and $U_2(x, y)$ are the light field in the planes immediately before and behind the LC lens, respectively, i.e. the coordinates on the front and back surfaces of the LC lens are the same: $x_1 = x_2 = x$, $y_1 = y_2 = y$, as shown in Fig. 27. In Eq. (33), the function $P(x, y)$ and the function $\delta(x, y)$ are the two functions responsible for the amplitude and phase in the incident light, respectively. The function $P(x, y)$ is sometimes called the pupil function of the lens and confined to the aperture of a lens. Assume the function $U_1(x, y) = 1$

which the uniform light source is incident upon the LC lens and the field in the observation

plane can be derived from the Fresnel diffraction formula, as shown in Eq. (34), [33]

$$U_3(x_3,y_3,z)=\frac{i\exp[-ikz]}{\lambda z}\int\int_{-\infty}^{\infty}U_2(x_2,y_2)\exp\left\{-\frac{ik}{2z}\left[(x_3-x_2)^2+(y_3-y_2)^2\right]\right\}dx_2dy_2,\qquad(34)$$

where $U_3(x_3,y_3)$, k and z are the field in the observation plane, the wave number $(2\pi/\lambda)$

and the distance between $U_2(x,y)$ and observation plane, respectively. Since the observation

plane of LC lens is not far away from the diffraction screen where the limitation is

$$z\le\frac{a^2}{\lambda},\qquad(35)$$

where a is the radius of effective aperture. As the principle in Fig. 28, the Fresnel diffraction

formula is used to calculate the Fresnel diffraction pattern in observation plane of LC lens.

Substituting Eq. (33) into Eq. (34) yields

$$\begin{aligned}U_3(x_3,y_3,z)&=\frac{i\exp[-ikz]}{\lambda z}\int\int_{-\infty}^{\infty}P(x,y)\exp[-i\delta(x,y)]\exp\left\{-\frac{ik}{2z}\left[(x_3-x)^2+(y_3-y)^2\right]\right\}dxdy\\&=\frac{i\exp[-ikz]}{\lambda z}\int\int_{-\infty}^{\infty}\left\{P(x,y)\exp[-i\delta(x,y)]\exp\left[-\frac{ik}{2z}(x_3^2+y_3^2)\right]\right.\\&\qquad\left.\exp\left[\frac{ik}{z}(x_3x+y_3y)\right]\exp\left[-\frac{ik(x^2+y^2)}{2z}\right]\right\}dxdy.\end{aligned}\qquad(36)$$

Assuming the LC lens is circularly symmetric and the pupil function is only a function of the

radial coordinate, i.e. $P(x,y)=P(r)$, where $r=(x^2+y^2)^{1/2}$, $r=r_2=(x_2^2+y_2^2)^{1/2}$ and $r_3=(x_3^2+y_3^2)^{1/2}$.

According to the assumption, Eq. (32) and Eq. (33) are simplified as followed,

$$\delta(r)=\frac{2\pi}{\lambda}\cdot\Delta n(r)\cdot d=k\left[n_{eff}(r)-n_{eff}(r)_{min}\right]\cdot d,\qquad(37)$$

$$U_2(r)=P(r)\exp[-i\delta(r)],\qquad(38)$$

where $n_{eff}(r)$ and $n_{eff}(r)_{min}$ are the effective index distribution of refraction and the

minimum of the effective index distribution of refraction, respectively. As the design of LC lens, the effective index distribution of refraction is an equation which would be designed as the GRIN Lens, as shown in below,

$$n_{eff}(r) = n_{eff}(r)_{max} - \varphi(r), \tag{39}$$

where $n_{eff}(r)_{max}$ and $\varphi(r)$ are the maximum of effective index distribution of refraction and the variation in distribution of refractive index, respectively. According to Eq. (39), the variation in distribution of refractive index is the function as below,

$$\varphi(r) = n_{eff}(r)_{max} - n_{eff}(r). \tag{40}$$

Substituting Eq. (37) and Eq. (39) into Eq. (38), the factor $\exp\{-ik[n_{eff}(r)_{max} - n_{eff}(r)_{min}]d\}$ represents a constant phase term contributed by a beam along the axis, so that it can be neglected as shown in below,

$$U_2(r) = P(r)\exp[i \cdot k \cdot \varphi(r) \cdot d]. \tag{41}$$

As the results, Eq. (36) is simplified by Eq. (40) and Eq. (41) as below,

$$U_3(r_3, z) = \frac{i\exp[-ikz]}{\lambda z}\exp\left[-\frac{ikr_3^2}{2z}\right]\int_0^a\int_0^{2\pi}\left\{P(r)\exp\left[ik[n_{eff}(r)_{max} - n_{eff}(r)]d\right]\right.$$
$$\left.\exp\left[\frac{ikr^2}{2}\left(-\frac{1}{z}\right)\right]\exp\left[\frac{ikrr_3}{z}\cos(\alpha-\beta)\right]\right\}\cdot rdrd\alpha, \tag{42}$$

where α and β are the angle of spherical coordinate in the plane of the aperture of LC lens and the plane of observation, respectively. In order to simplify Eq. (42), the Hankel transform is used to do it as below,

$$J_0(\eta) = \frac{1}{2\pi}\int_0^{2\pi}e^{i\cdot\eta\cdot\cos\zeta}d\zeta, \tag{43}$$

where J_0 is a Bessel function of the first kind of order zero. Because of the complete axial

symmetry, the solution must be independent of β. Based on the reason, Eq. (46) would may as well to solve by $\beta = 0$, the deriving result is

$$U_3\left(r_3,z\right) == \frac{i\exp\left[-ikz\right]}{\lambda z}\exp\left[-\frac{ikr_3^2}{2z}\right]\int_0^a\left\{P(r)\exp\left[ik\left[n_{eff}(r)_{\max}-n_{eff}(r)\right]d\right]\right.$$
$$\left.\exp\left[\frac{ikr^2}{2}\left(-\frac{1}{z}\right)\right]J_0\left(\frac{krr_3}{z}\right)\right\}\cdot 2\pi\cdot rdr.$$ (44)

Assuming the parameters of v, u, N and ρ are the radial coordinate, the axial coordinate, Fresnel number and the normalized radial coordinate over the lens aperture, respectively as followed,

$$v = \frac{2\pi}{\lambda}\frac{a}{z}r_3,$$ (45)

$$u = \frac{2\pi}{\lambda}a^2\left(\frac{1}{z}\right),$$ (46)

$$N = \frac{a^2}{\lambda z},$$ (47)

$$\rho = \frac{r}{a}, P(\rho) = \begin{cases} 1, \rho \leq 1 \\ 0, \rho > 1 \end{cases},$$ (48)

where a is the radius of the effective aperture of LC lens. According to the above definitions Eq. (45-48), Eq. (44) is simplified by substituting from Eq. (45) to Eq. (48) into Eq. (44) as below,

$$U_3\left(v,u\right) = 2\pi iN\exp\left[-ikz\right]\exp\left[-\frac{iv^2}{4\pi N}\right]\int_0^1\left\{\exp\left[ik\left[n_{eff}(\rho)_{\max}-n_{eff}(\rho)\right]d\right]\right.$$
$$\left.\exp\left[\frac{iu\rho^2}{2}\right]J_0\left(v\rho\right)\right\}\cdot \rho d\rho.$$ (49)

According to the deriving of above-mentioned results, the irradiance distribution of LC lens is calculated as below, and the PSF of LC lens is defined from the result of irradiance distribution of LC lens,

$$PSF(v,u) \equiv I(v,u) = |U_3(v,u)|^2 \,. \tag{50}$$

By the deriving of irradiance distribution of LC lens, the PSF of LC lens is calculated by given any position of observation plane in Eq. (49). According to the result of PSF, the observation plane of LC lens which has the highest relative irradiance peak is determined.

4.2 Modulation Transfer Function of the Liquid Crystal Lens by Modulation

Generally speaking that the object passes through the LC lens the image is formed in the observation plane or focal plane. As the result, to develop the quantitative imaging quality is the most important and indispensable task for the LC lens. The quantitative imaging quality is generally using modulation transfer function (MTF) to assess the focusing quality of an optical lens. According to the assessment of MTF, the quantitative imaging quality of LC lens is also used MTF to assess. Moreover, the assessment of MTF is used to optimize the design of LC lens before realization by the processes of optimization. In addition, the assessment of MTF is developed by the method of modulation in this study which the method is calculated by convolution (denoted by $\otimes$). The method of modulation to calculate MTF is that uses the on-axis point spread function (PSF) to convolve the object.

This fact has led to the widespread use of the modulation transfer function (MTF) to describe the performance of a lens system. A type of target commonly used to test the performance of an optical system consist of a series of alternating bright and dark bars of equal width, as shown in Fig. 28(a). Several sets of patterns of different spacing are usually imaged by the system under test and the finest set in which the line structure can be discerned is considered to be the limit of resolution of the system, which is expressed as a certain number of lines per millimeter (Lp/mm). A cross section of the brightness of the bar objects is shown in Fig. 28(b) and Fig. 29 shows how the image is calculated by the operation of convolution (denoted by $\otimes$), i.e. $Object \otimes PSF = Image$. In Fig. 30, the effect of the image

blur on progressively finer patterns is indicated. It is apparent that when the illumination contrast in the image is less than the smallest amount that the system (e.g., the eye film or photodetector) can detect, the pattern can no longer be resolved. If the contrast in the image as a "modulation" is expressed, given by the Eq. (51), [34]

$$\text{Modulation} = \frac{A_{max} - A_{min}}{A_{max} + A_{min}}, \tag{51}$$

where A_{max} and A_{min} are the image illumination levels (amplitude levels) as indicated in Fig. 30, the modulation as a function of the number of lines per millimeter (Lp/mm) in the image is plotted. The preceding discussion has been based on patterns whose brightness distribution is a square wave (Fig. 28(b)) and whose image illumination distribution is distorted by characteristics of the optical system, as shown in Fig. 30. In addition, if the object pattern brightness distribution is in the form of a sine wave, regardless of the shape of the spread function. The MTF to describe the performance of a lens system is the ratio of the modulation in the image that the object is as a function of the frequency (cycles per unit of length) of the sine-wave pattern. Therefore, the MTF as the ratio is calculated in percent by Eq. (52), Eq. (53) and Eq. (54),

$$M_o = \frac{A_{o\,max} - A_{o\,min}}{A_{o\,max} + A_{o\,min}}, \tag{52}$$

$$M_i = \frac{A_{i\,max} - A_{i\,min}}{A_{i\,max} + A_{i\,min}}, \tag{53}$$

$$\text{MTF(\%)} = \frac{M_i}{M_o} \times 100\%, \tag{54}$$

where $A_{o\,max}$, $A_{o\,min}$, M_o and $A_{i\,max}$, $A_{i\,min}$, M_i are the maximum amplitude of the object, the minimum amplitude of the object, the modulation depth of the object and the maximum amplitude of the image, the minimum amplitude of the image, the modulation depth of the image, respectively. Moreover, the different line pair objects are convolved with the PSF of

LC lens, and their performance of image is shown in the observation plane or focal plane. According to the above-mentioned calculation, the quantitative imaging quality of LC lens based on MTF is developed.

4.3 Simulation Verification

4.3.1 The Structure of Liquid Crystal Lens

The simulations of LC lens in this study are conducted for the LC lens with the hole-type electrode that the diameter of effective aperture and the length of square shape are 3mm and 20mm respectively in our laboratory, as shown in Fig. 31. The materials of electrode are all ITO glass, and the glass is general glass with dielectric constant $\varepsilon_{glass} = 6.9$ in this study. The other specifications in this study are shown in Table 29, respectively. The top ITO electrode is used to prevent the disclination by two voltages driving in experiment. The driving method is given the voltage to the up ITO electrode about 5 seconds first, and then opens it to turn the voltage to the hole-pattern ITO electrode. Therefore, the defect of disclination would not occur to affect the performance in experiment. Since the method of two voltages driving in simulation by the software of $2\text{dimMOS}^{\text{TM}}$ would not be realized that the top ITO electrode would not be opened at same time, the defect of disclination would occur in simulation. According to the structure and specifications of the LC lens with the hole-type electrode in our laboratory, the hole-pattern ITO electrode is given the applied voltage from $10V_{\text{rms}}$ to $50V_{\text{rms}}$ in $5V_{\text{rms}}$ steps in this study. As the simulation of dynamic LC molecules is obtained the tilt angle θ by using the software of $2\text{dimMOS}^{\text{TM}}$. As the results of simulation, the effective index distribution of refractive $n_{\text{eff}}(r)$ of the LC lens with the hole-type electrode in our laboratory by given the applied voltage from $10V_{\text{rms}}$ to $50V_{\text{rms}}$ in $5V_{\text{rms}}$ steps are calculated by the method of integration in Eq. (31) in this study, respectively. By given the

applied voltage form $10V_{rms}$ to $50V_{rms}$ in $5V_{rms}$ steps for the LC lens with the hole-type electrode in our laboratory, the calculating results of effective index distribution of refractive $n_{eff}(r)$ are shown in Fig. 32 respectively. In Fig. 32, the defect of disclination is occurring of the LC lens with the hole-type electrode in our laboratory by given the applied voltage from $35V_{rms}$ to $50V_{rms}$.

4.3.2 The Point Spread Function and the Modulation Transfer Function of the Liquid Crystal Lens

In order to simulate and calculate the PSF and MTF of LC lens, the effective index distribution of refractive $n_{eff}(r)$ has to determine first. By given the applied voltage form $10V_{rms}$ to $50V_{rms}$ in $5V_{rms}$ steps for the LC lens with the hole-type electrode in our laboratory, the calculating results of effective index distribution of refractive $n_{eff}(r)$ are shown in Fig. 32. Based on the effective index distribution of refractive $n_{eff}(r)$ of the LC lens, the irradiance distribution as the PSF is calculated by Eq. (49) and Eq. (50) as shown in Fig. 33, where the results of PSF for the LC lens with the hole-type electrode by given the applied voltage form $10V_{rms}$ to $50V_{rms}$ in $5V_{rms}$ steps in our laboratory in its observation plane has the highest peak of relative intensity. It could be found that the distribution is narrowed to small area while the applied voltage increased. As the results of PSF, the MTFs of the LC lens are calculated, as shown in Fig. 34.

5 Optimal Design of the Liquid Crystal Lens with Multi-ring Electrodes

According to the theories for LC lens in section 4 of PSF and MTF, the quantitative imaging quality of the LC lens with multi-ring electrodes in different layers is assessed. According to the quantitative imaging quality, the design of the LC lens with the number of ring electrodes is optimized. The optimal design is that the LC lens has the minimum number of ring electrodes, and its imaging quality is not increased significantly even with more number of ring electrodes. As the shown in Fig. 26, the effective index distribution of refractive $n_{eff}(r)$ of the LC lens with the number of ring electrodes from two to seven rings in different layers is compared with the LC lens only with the first ring electrode, and the LC lens with multi-ring electrodes in different layers improves the defects of the LC lens with the hole-type electrode in our laboratory that includes the weak distribution of electric field at the center in the LC layer, the unlike distribution of effective index of refraction at the center of the LC lens, and the disclination occurring by given voltage. Based on the effective index distribution of refractive $n_{eff}(r)$ as shown in Fig. 26, the irradiance distribution as the PSF is calculated by Eq. (49) and Eq. (50) as shown in Fig. 35, where the results of PSF for the LC lens with the number of ring electrodes from two to seven rings in different layers in its observation plane has the highest peak of relative intensity. According to the PSF of the LC lens with the number of ring electrodes from two to seven rings in different layers, the MTF is calculated by the theories of modulation as shown in Fig. 36. As the results of MTF corresponding to 5 and 7 line pairs per millimeter (donated Lp/mm) in Fig. 36, the assessment of imaging quality for the LC lens with the number of ring electrodes from two to seven rings in different layers is illustrated in Fig. 37 and Fig. 38 respectively, where the observation plane is in its highest relative intensity peak of PSF.

The results of MTF by modulation which the observation plane is in its highest relative intensity peak of PSF, the imaging quality for ideal results should be increased with that the number of ring electrodes of the LC lens is also increased. As the illustrations in Fig. 37 and Fig. 38, the numerical value of MTF corresponding to $5\,\mathrm{Lp/mm}$ and $7\,\mathrm{Lp/mm}$ for some design of the LC lens with the number of ring electrodes from two to seven rings in different layers are not perfect fitting for the ideal results, however the trend of the results is the same with the ideal results. Since the optimal design of the LC lens with multi-ring electrodes in different layers is determined by the imaging quality based on PSF and MTF, the optimal design is that the LC lens has the minimum number of ring electrodes, and its imaging quality is not increased significantly even with more number of ring electrodes. As the illustrations in Fig. 35 and Fig. 37-38, the profile of PSF and the numerical value of MTF corresponding to $5\,\mathrm{Lp/mm}$ and $7\,\mathrm{Lp/mm}$ are shown that the LC lens with three-ring electrodes in different layers is the minimum number of ring electrodes, and its imaging quality is not increased significantly even with the ring number increased to seven. Consequently, the optimal design of the LC lens with multi-ring electrodes in different layers is designed as three-ring electrodes with the specifications of effective focal length and the diameter of effective aperture as 112mm and 3mm.
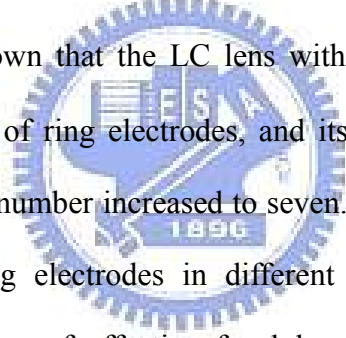
6 Conclusions and Future Works

A liquid crystal (LC) lens replacing the moving lenses in the auto-focusing (AF) and zooming systems for the cameras in cell phones are designed and optimized in this study. In results, the thickness of lens modules can be significantly reduced to be implemented in compact cell phones. This LC lens owns multi-ring electrodes to generate non-uniform electric field for focusing. Since the results of design are based on the simulation by using the software package 2dimMOS^{TM}, the thickness of LC layer and electrode would result in the difference between simulation and reality. The image quality of the designed LC lens is assessed by developing a new evaluation method based on point spread function (PSF) and modulation transfer function (MTF) of the focusing. Based the calculated PSF and MTF, the electrode widths are optimized to render the best imaging quality in terms of MTFs. Since the calculation of PSF and MTF are depended on the wave length of light, the results of optimization would be affected. Based on the results obtained in the previous sections, the following conclusions can be drawn.

(1) The designed LC lens is proven effective to replace the moving lenses in the traditional AF and/or zooming module to reduce the overall thickness, in order to implement in cell phones.

(2) The non-uniform electric field desired for focusing is successfully generated by multi-ring electrodes designed in the structure of the newly-developed LC lens.

(3) The assessment method for image quality is also successfully developed via MTF by the calculating method of modulation, based on which the electrode widths are optimized to reach a satisfactory imaging quality and simultaneously small number of electrodes. It is suggested that the number of ring electrodes is designed to be three to reach MTF of 65% for 5 and 48% for 7 line pairs per millimeter, since the MTF would not be increased

significantly even with the electrode number is increased to seven.

In the future, the electrode should be designed as non-planar ones for implementation, in order to realize the voltage application. Furthermore, a concrete theoretical computation procedure would be developed to obtain precise electrode widths. Moreover, the PSF and MTF should consider the aberration of the LC lens, in order to assess the focusing quality precisely.

References

[1] J.S. Lee, Y.Y. Jung, B.S. Kim, and S.J. Ko, "An advanced video camera system with robust AF, AE, and AWB control," *IEEE Transactions on Consumer Electronics*, v 47, n 3, pp. 694-699 (2001).

[2] J.S. Lee, S.J. Ko, Y. Kim, and A. Morales, "A video camera system with adaptive zoom tracking," *International Conference on Consumer Electronics*, pp. 56-57 (2002).

[3] S.Y. Lee, S.S. Park, and C.S. Kim, "Low-power Auto Focus Algorithm Using Modified DCT for Mobile Phones," *International Conference on Consumer Electronics*, pp. 67-68 (2006).

[4] S. Sato, "Liquid-crystal lens-cells with variable focal length," *Japanese Journal of Applied Physics*, v 18, n 9, pp. 1679-1684 (Sep. 1979).

[5] M. Honma, S. Masuda, T. Nose, and S. Sato, "Optical properties of an anamorphic liquid crystal microlens using an elliptically-patterned electrode structure," *Proceedings of SPIE – The International Society for Optical Engineering*, v 3143, pp. 208-213 (1997).

[6] M. Ye and S. Sato, "Optical properties of liquid crystal lens of any size," *Japanese Journal of Applied Physics*, v 41, n 5B, pp. 571-573 (May 2002).

[7] M. Ye, B. Wang, and S. Sato, " Liquid-crystal lens with a focal length is variable in a wide range," *Optical Society of America*, v 43, n 35, pp. 6407-6412 (Dec. 2004).

[8] B. Wang, M. Honma, T. Nose, and S. Sato, "Liquid crystal lens with spherical electrode," *Japanese Journal of Applied Physics*, v 41, n 11A, pp. 1232-1233 (Nov. 2002).

[9] B. Wang, M. Ye, and S. Sato, "Study on Liquid Lens with Curved Electrode," *Proceedings of SPIE*, v 6018 (2005).

[10] B. Wang, M. Ye, and S. Sato, "Lens of electrically controllable focal length made by a glass lens and liquid-crystal layers," *Applied Optics*, v 43, n 17, pp. 3420-3425 (Jun. 2004).

[11] H. Ren, Y.-H. Fan, S. Gauza, and S.-T. Wu, "Tunable-focus flat liquid crystal spherical lens," *Applied Physics Letters*, v 84, n 23, pp. 4789-4791 (Jun. 2004).

[12] H. Ren and S.-T. Wu, "Adaptive liquid crystal lens with large focal length tunability," *Optical Society of America*, v 14, n 23 (Nov. 2006).

[13] M. Ye, B. Wang, and S. Sato, "Double-layer liquid crystal lens," *Japanese Journal of Applied Physics*, v 43, n 3A, pp. 352-354 (Feb. 2004).

[14] B. Wang, M. Ye, and S. Sato, "Liquid crystal lens woth stacked structure of liquid-crystal layers," *Optical Communications*, v 250, pp.266-273 (Feb. 2005).

[15] H. Ren, Y.-H. Fan, S. Gauza, and S.-T. Wu, "Tunable-focus cylindrical liquid crystal lens," *Japanese Journal of Applied Physics*, v 43, n 2, pp. 652-653 (Feb. 2004).

[16] H. Ren, Y.-H. Lin, and S.-T. Wu, "Adaptive lens using liquid crystal concentration redistribution," *Applied Physics Letters*, v 88, n 19 (May 2006).

[17] B. Wang, M. Ye, and S. Sato, "Liquid crystal negative lens," *Japanese Journal of Applied Physics*, v44, n 7A, pp. 4979-4983 (Jul. 2005).

[18] T. Takahashi, M. Ye, and S. Sato, "Wavefront Aberrations of a Liquid Crystal Lens with focal Length Variable form Negative to Positive Values," *Japanese Journal of Applied Physics*, v46, n 5A, pp. 2926-2931 (May. 2007).

[19] B. Wang, M. Ye, and S. Sato, "Liquid crystal lens with focal length variable from negative to positive values," *IEEE Photonics Technology Letters*, v 18, n 1,pp. 79-81 (Jan. 2006).

[20] M. Ye, B. Wang, and S. Sato, "Driving of liquid crystal lens without disclination occurring by applying in-plane electric field," *Japanese Journal of Applied Physics*, v 42, n 8, pp. 5086-5089 (Aug. 2003).

[21] Z. He, T. Nose and S. Sato, "Optical Performance of Liquid Crystal Cells with Asymmetric Silt-Patterned Electrodes in Various Applied Field Configurations," *Japanese Journal of Applied Physics*, v33, n 2, pp. 1091-1095 (Feb. 1994).

[22] M. Ye, B. Wang, and S. Sato, "Liquid Crystal Lens Driven by Two voltages", *Proceedings of SPIE*, v 6018 (2005).

[23] M. Ye and S. Sato, "Two-dimensional focus control for liquid crystal lens," *Proceedings of SPIE*, v 5213.

[24] M. Ye and S. Sato, "Liquid crystal lens with focus movable along and off axis," *Optical Communications*, v 225, pp. 227-280 (Jul. 2003).

[25] M. Ye, B. Wang, and S. Sato, "Study of Liquid Crystal Lens with Focus Movable in Focal Plane by Wave Front Analysis," *Japanese Journal of Applied Physics*, v45, n 8A, pp. 6320-6322 (Aug. 2006).

[26] M. Ye, B. Wang, and S. Sato, "Liquid crystal lens with focus movable in focal plane," *Optical Communications*, v 259, pp. 710-722 (Sep. 2005).

[27] P.-C. Chen, "Optical automatic focuses adjustment system for zoom lens," *National Central University, Department of Optics and Photonics* (Jun. 2004).

[28] Largan Precision Co., Ltd, http://www.largan.com.tw/.

[29] M. Katz, Introduction to Geometrical Optics, *World Scientific* (2002).

[30] E. Hecht, Optics (Fourth Edition), *Addison Wesley* (2002).

[31] H. J. Deuling, "Deformation of Nematic Liquid Crystals in an Electric Field," *Molecular Crystals and Liquid Crystals*, v 19, pp. 123-131 (Feb. 1972).

[32] E. Lueder, Liquid Crystal Displays, *John Wiley & Sons Ltd* (2001).

[33] M. Gu, Advanced Optical Imaging Theory, *Springer* (2000).

[34] G. D. Boreman, Modulation Transfer Function in Optical and Electro-Optical Systems, *SPIE PRESS* (2001).

Figures
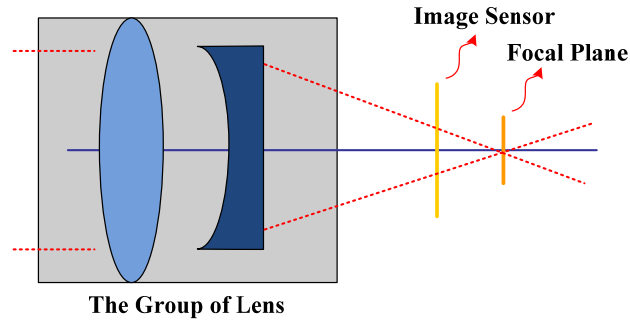
Fig. 1 The traditional AF system.
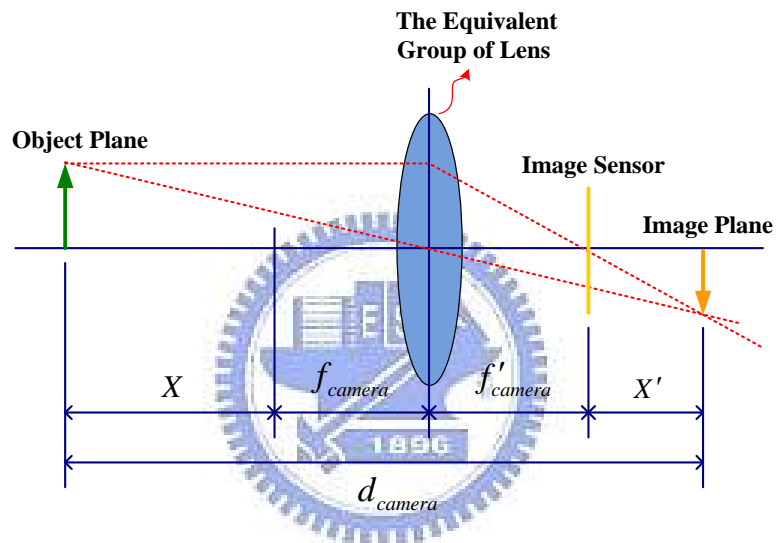
Fig. 2 The illustration shows the relative parameters of the traditional AF system.
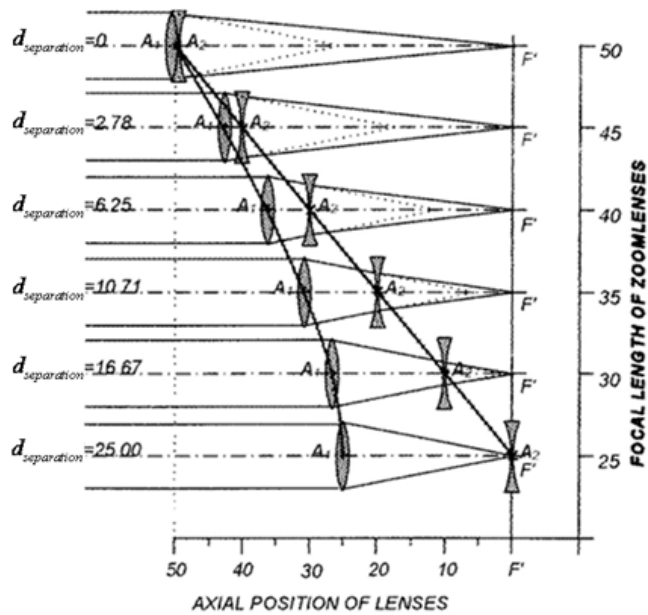
Fig. 3 The traditional zooming system. [28]
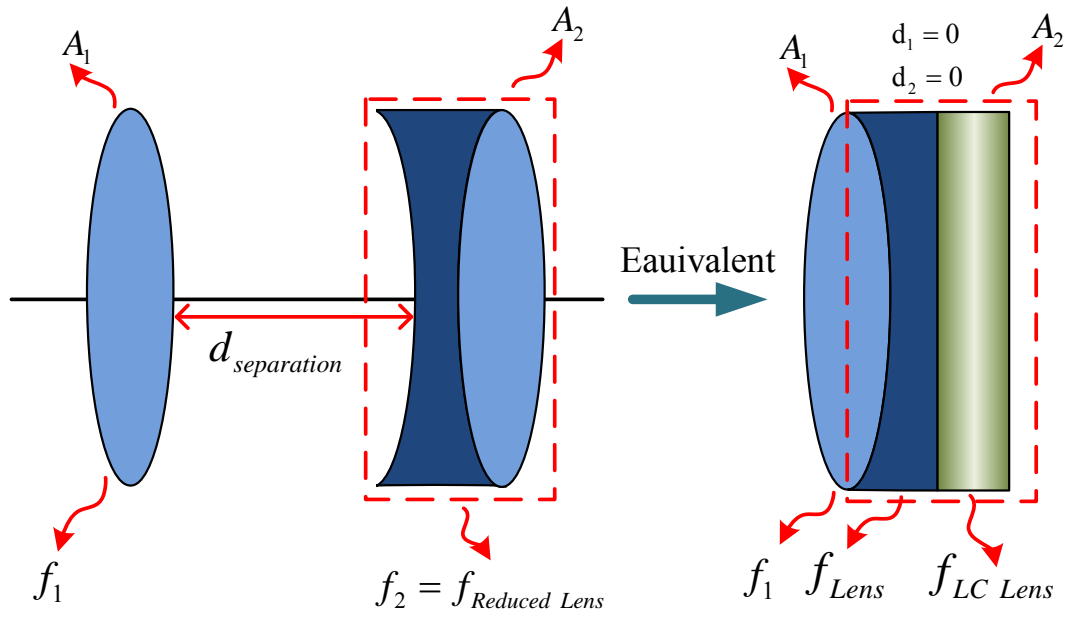
Fig. 4 The zooming system including positive LC lens.
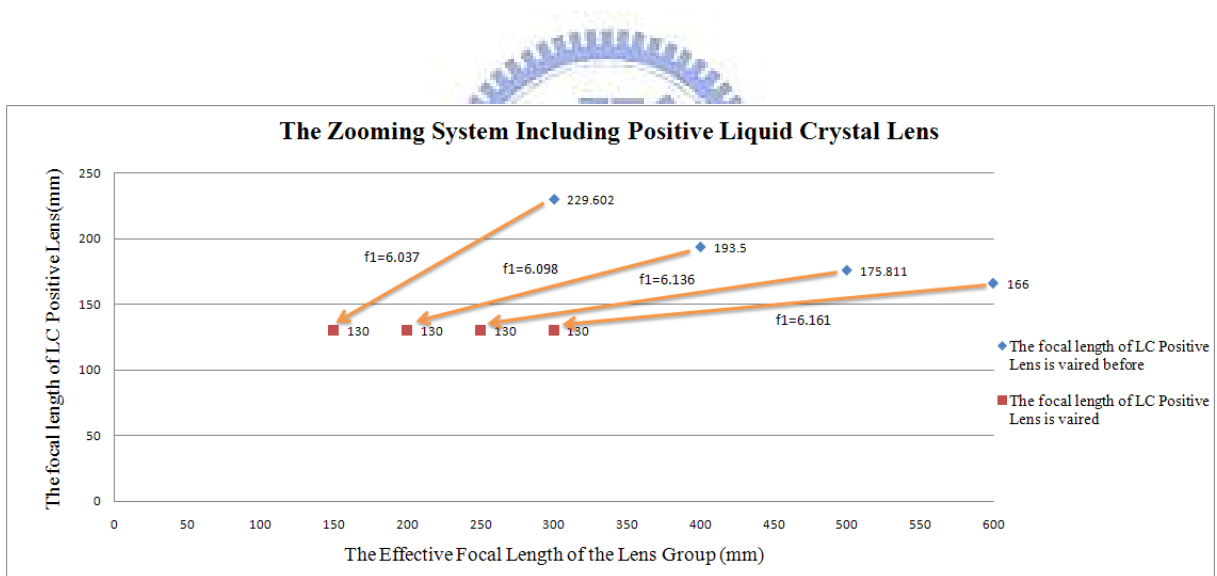
Fig. 5 The illustration shows the function of zooming by a positive LC lens.
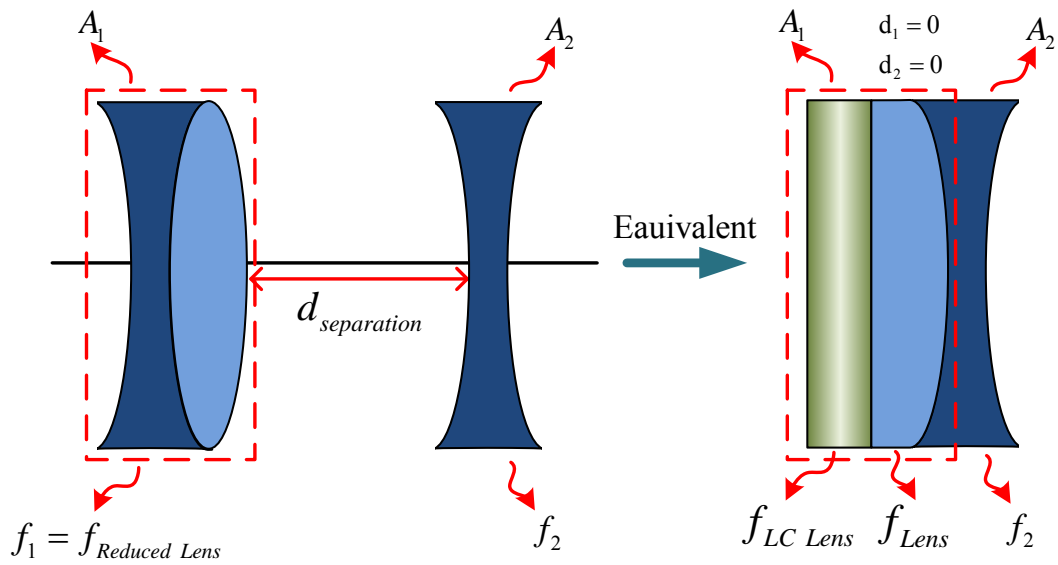
Fig.6 The zooming system including negative LC lens.
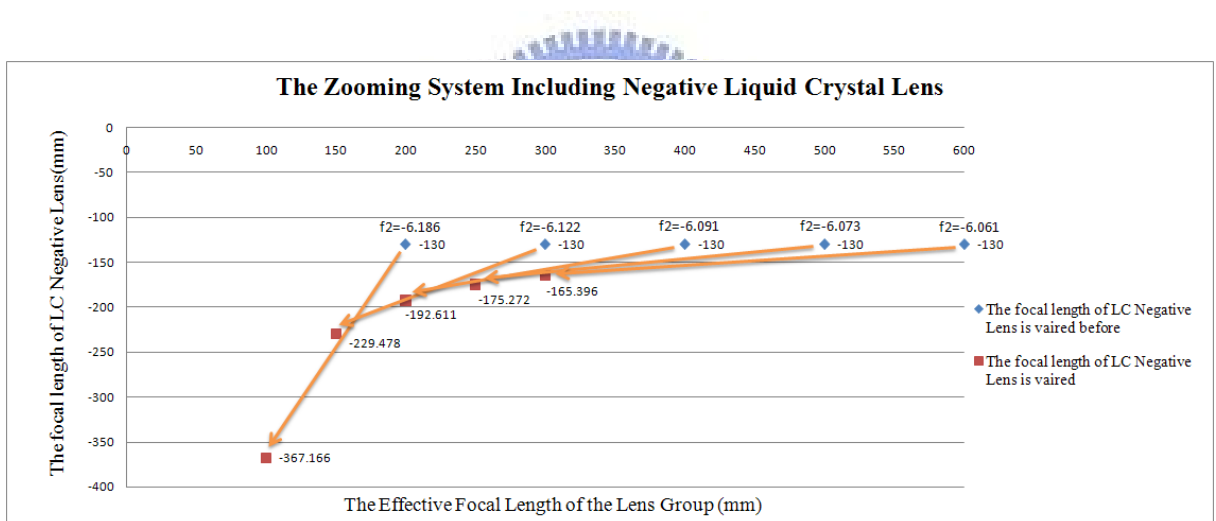
Fig.7 The illustration shows the function of zooming by a negative LC lens.
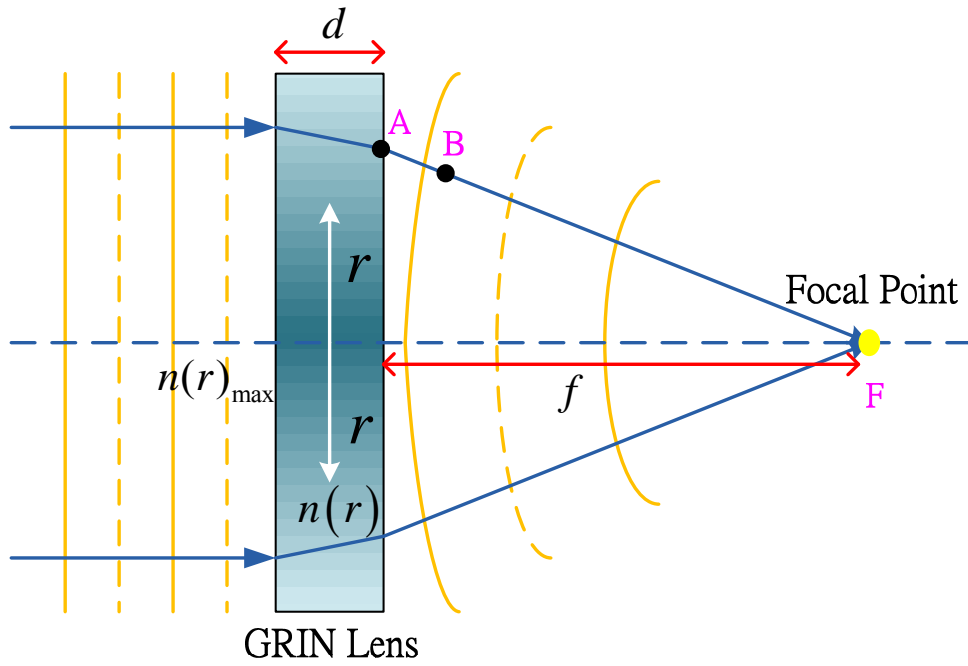
Fig. 8 The geometry corresponds to the focusing of parallel rays by a GRIN lens.
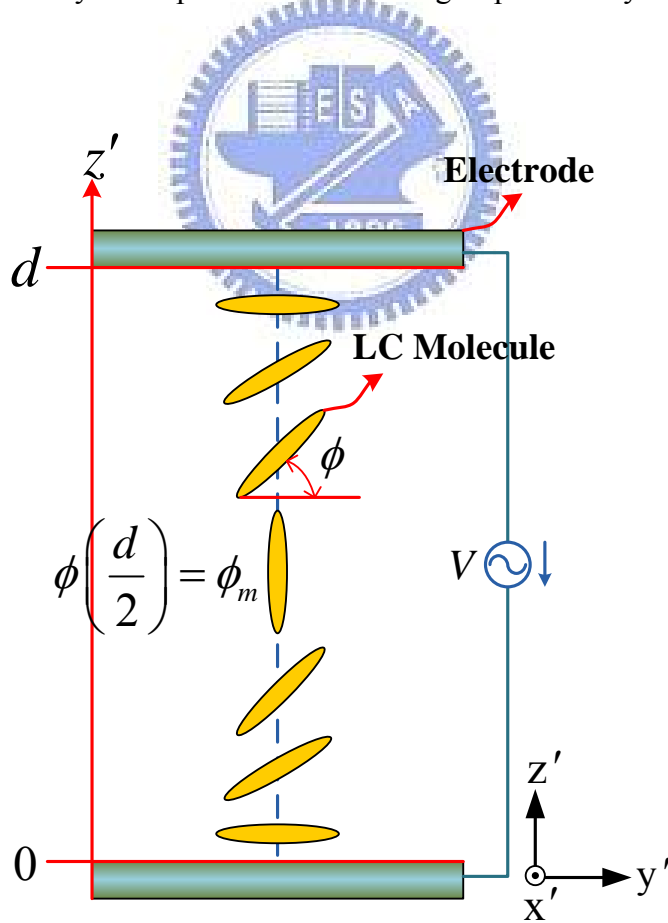
Fig. 9 The orientation model for nematic liquid crystal molecules rise from the substrate by the electric field.
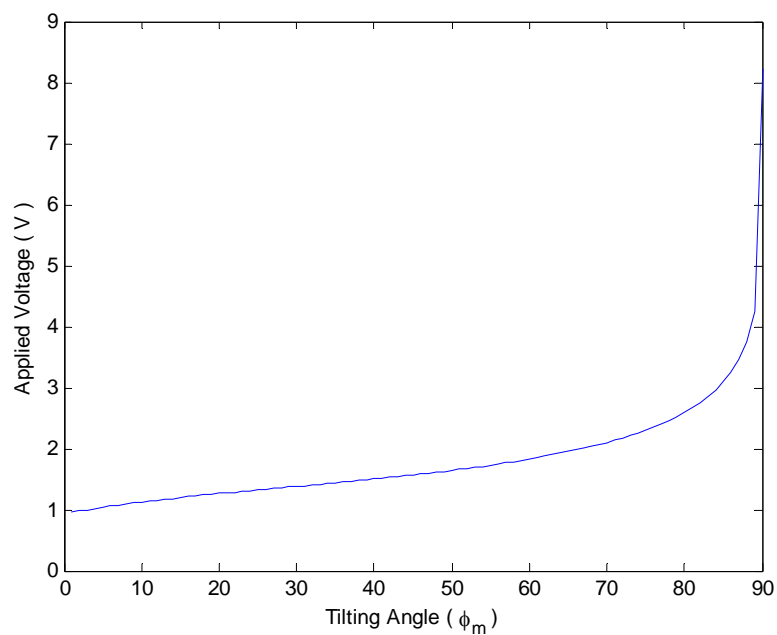
Fig. 10 The relation between the applied voltage V and the maximum tilting angle ϕ_m.
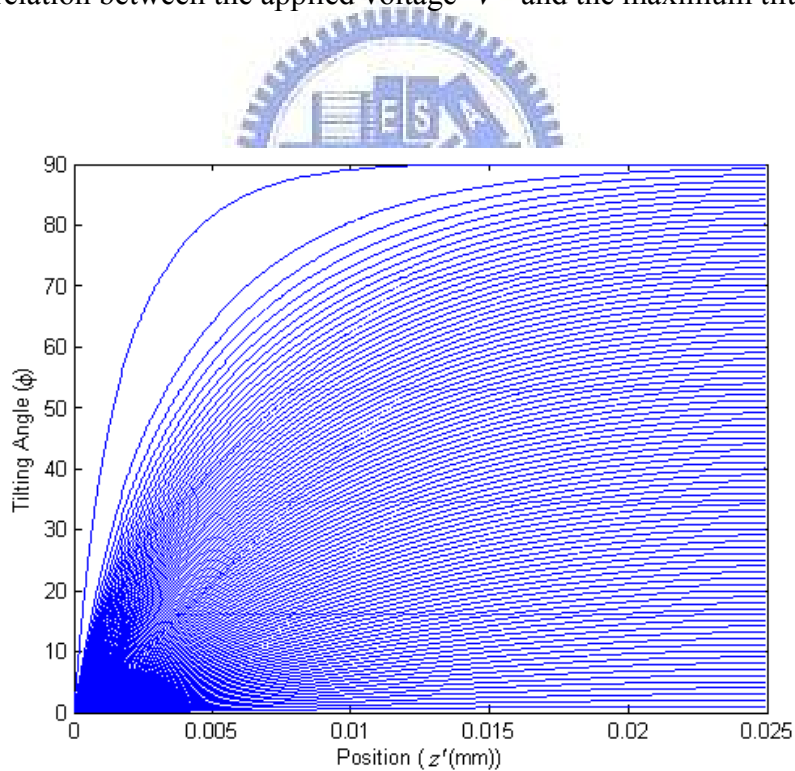
Fig. 11 The relation between the tilting angle ϕ and the position in coordinate z'.
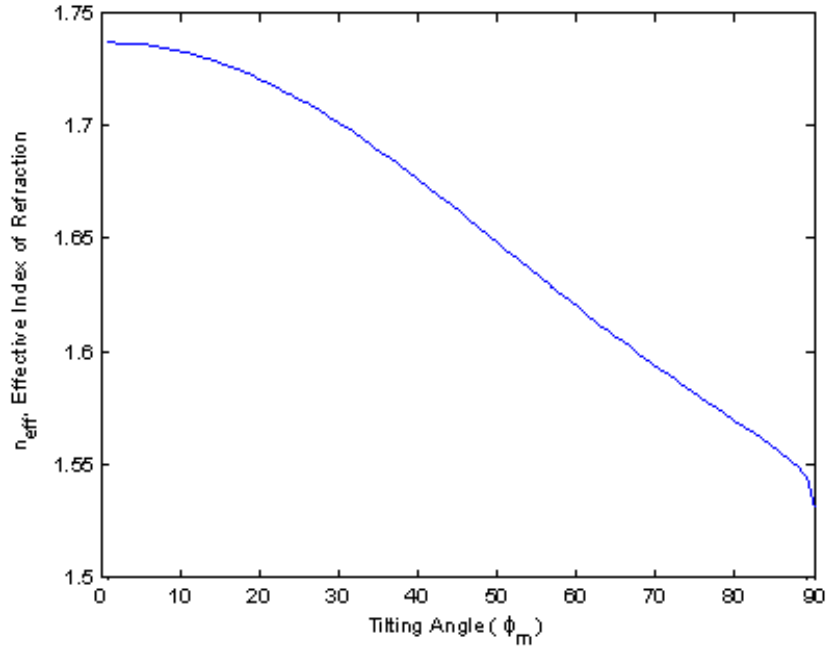
Fig. 12 The relation between the effective index of refraction n_{eff} and the maximum tilting

angle ϕ_m.
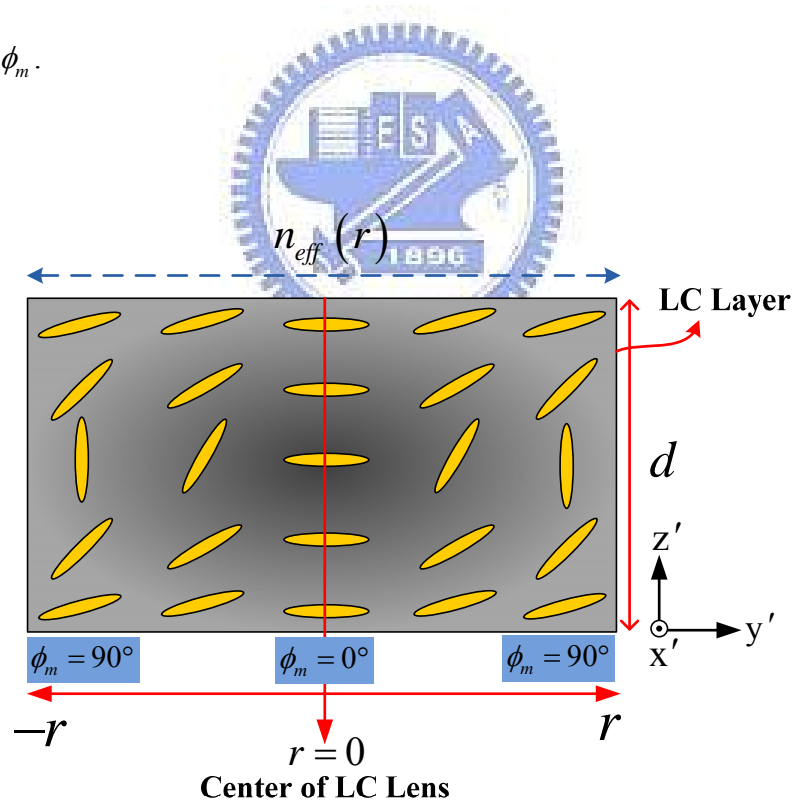
Fig. 13 The effective index distribution of refraction $n_{eff}(r)$ corresponds to the maximum

tilting angle ϕ_m from center to the radius r of effective aperture

(ϕ_m from 0° to 90°).
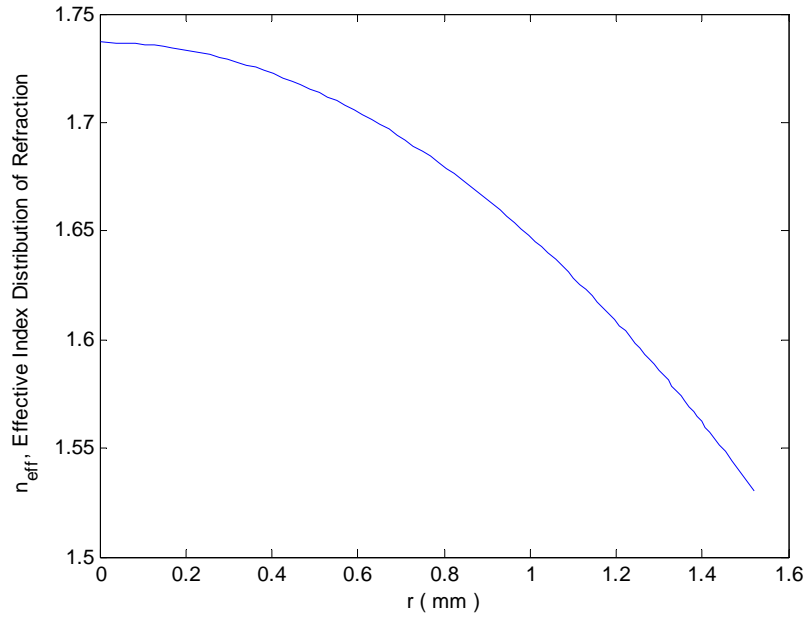
Fig. 14 The relation between the effective index distribution of refraction $n_{eff}(r)$ and the

radius r of effective aperture of the LC lens with multi-ring electrodes is given the

focal length 112mm.
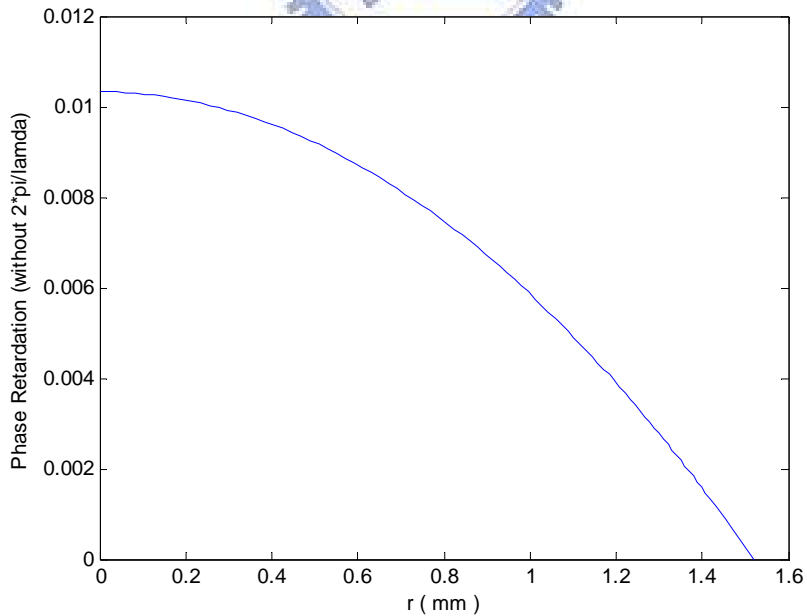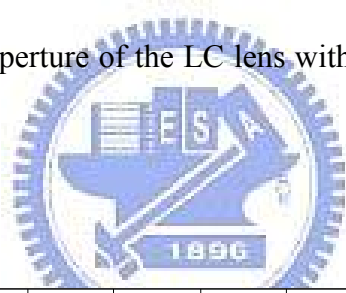
Fig. 15 The relation between the phase retardation $\delta(r)$ and the radius r of effective

aperture of the LC lens with multi-ring electrodes lens is given the focal length

112mm.
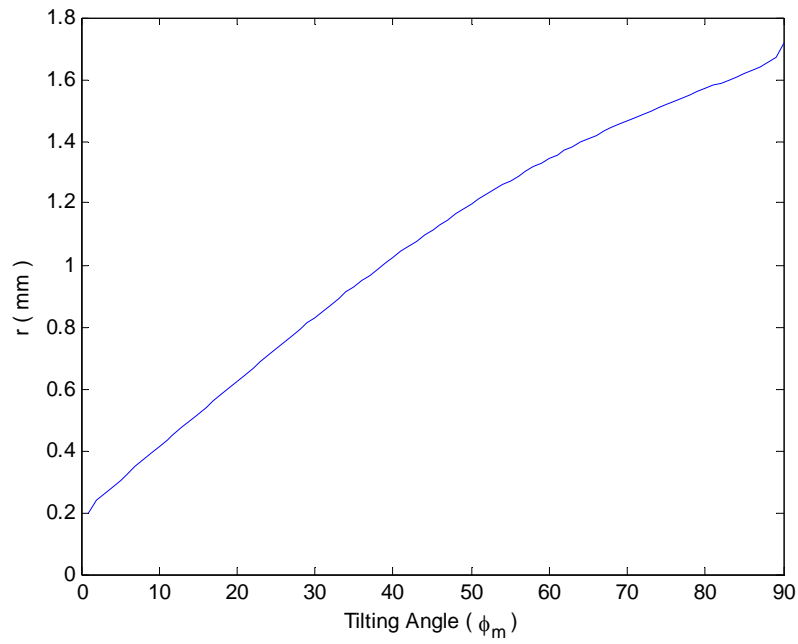
Fig. 16 The relation between the radius r of effective aperture and the maximum tilting

angle ϕ_m .
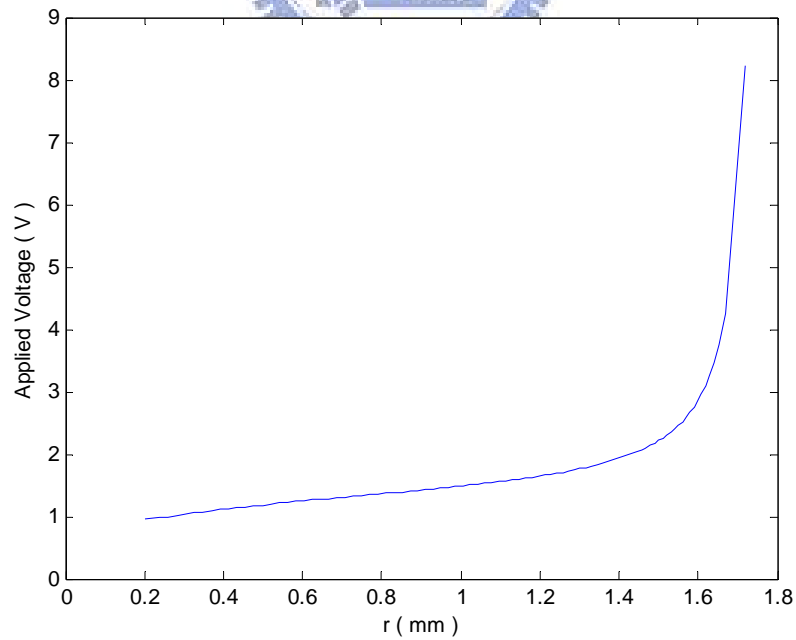
Fig. 17 The relation between the applied voltage V and the radius r of effective aperture.
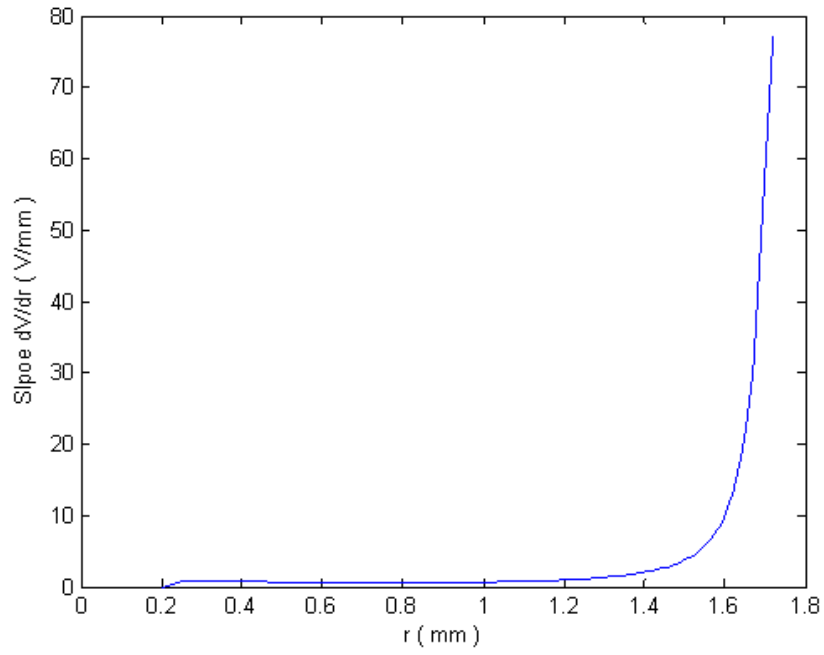
Fig. 18 The relation between the slope of $V(r)$ and the radius r of effective aperture.
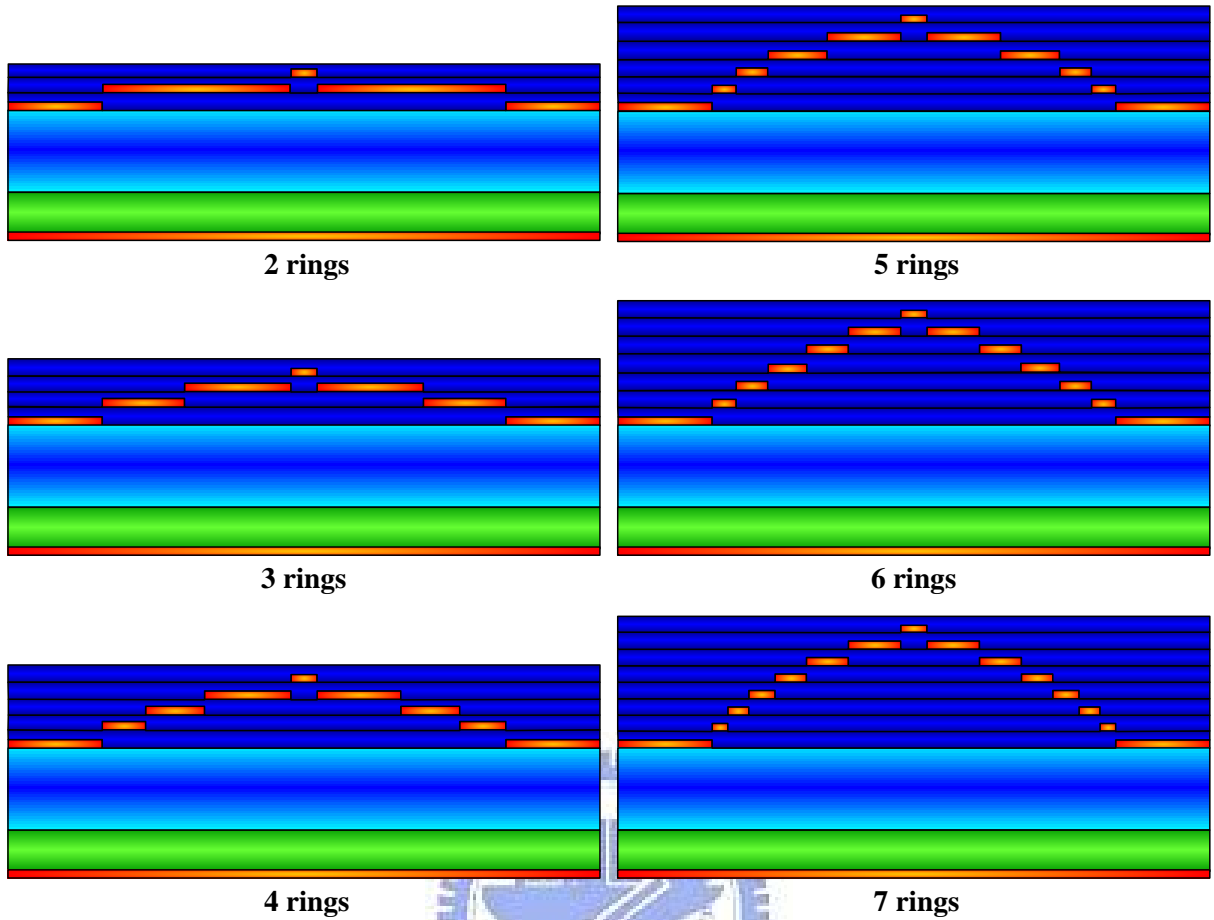
2 rings   **5 rings**

3 rings   **6 rings**

4 rings   **7 rings**

Fig. 19   The LC lens with the number of ring electrodes from two to seven rings in different layers.
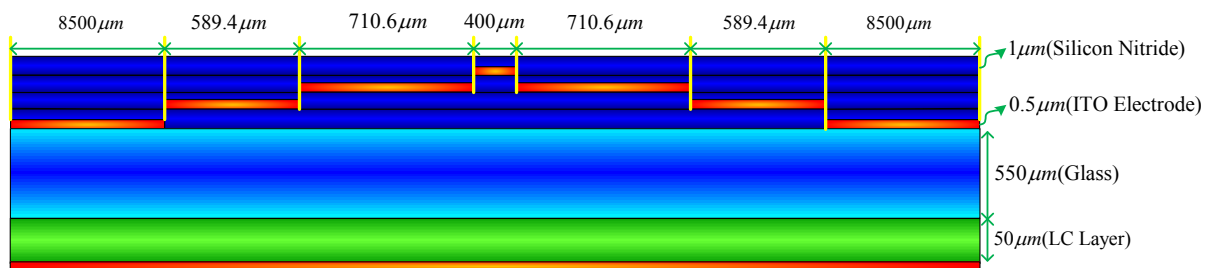
Fig. 20   The relative thicknesses and materials of the LC lens with three-ring electrodes in different layers.
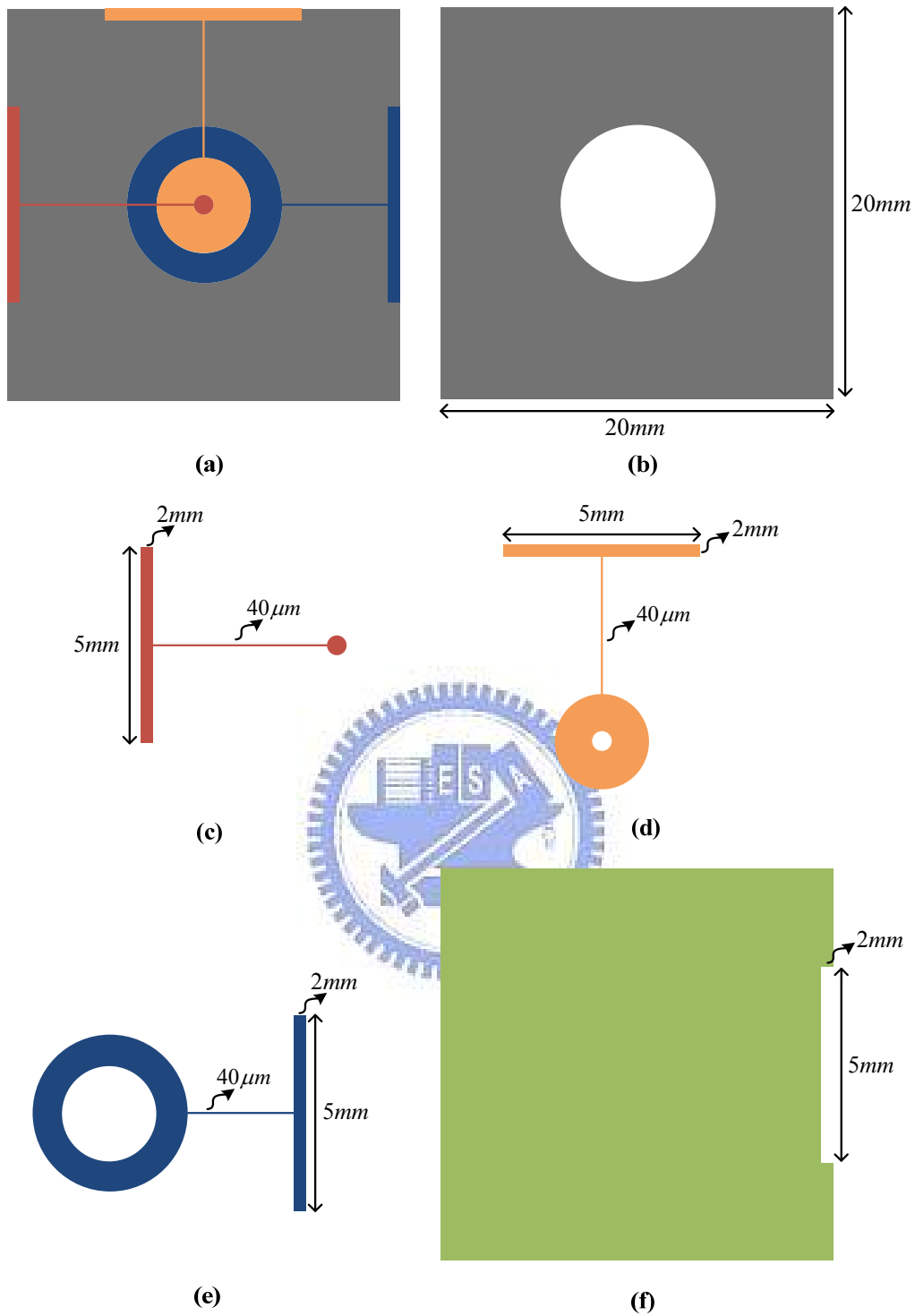
Fig. 21 The structure of the LC lens with three-ring electrodes in different layers: (a) the upper view of the LC lens; (b) the hole-type electrode of the LC lens; (c) the first ring electrode of the LC lens; (d) the second ring electrode of the LC lens; (e) the third ring electrode of the LC lens; (f) the photo mask to expose the conducting plates of the LC lens.
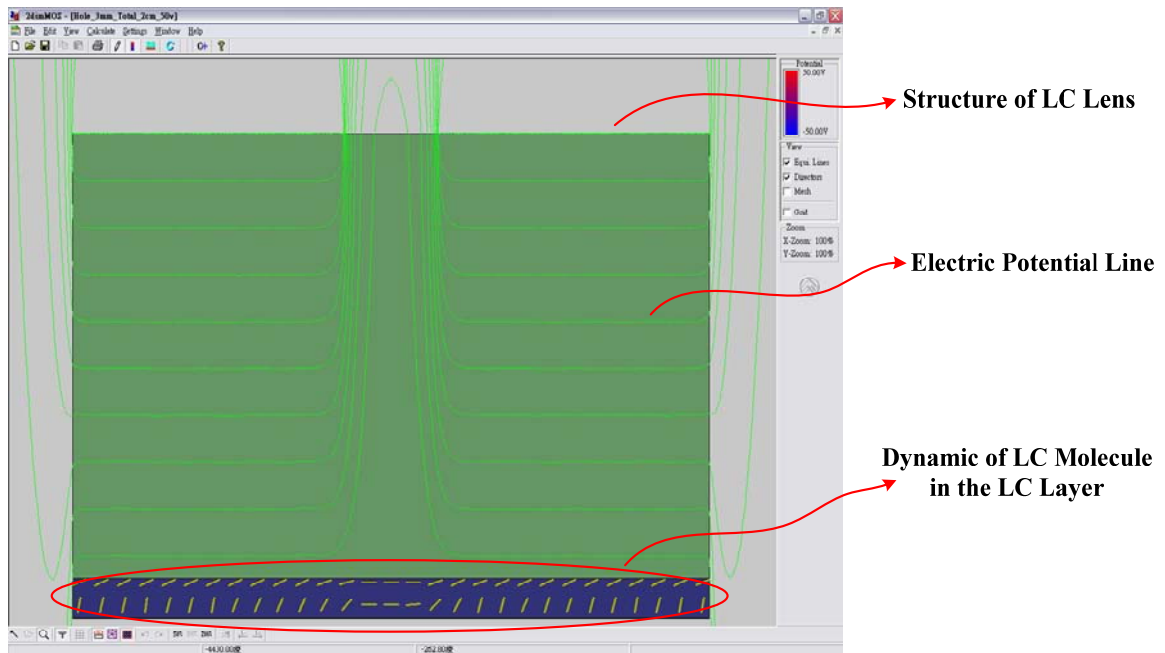
Fig. 22 The software package 2dimMOS^{TM} from Autronic-Melchers is used to simulate the

dynamic LC molecules in LC lens.
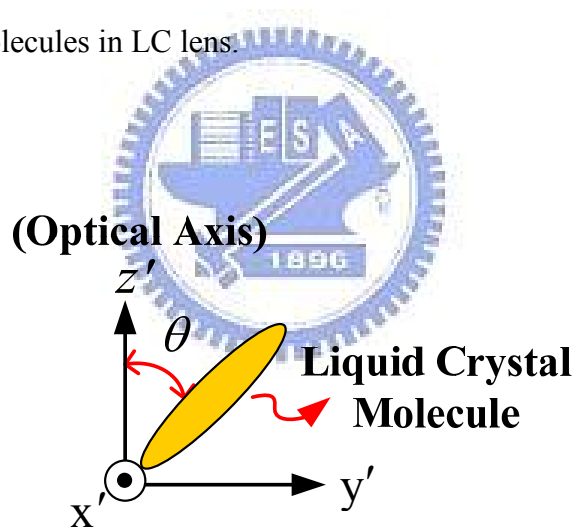
Fig. 23 The coordinate of LC molecule and tilting angle θ between the liquid crystal

molecule and optical axis z' .
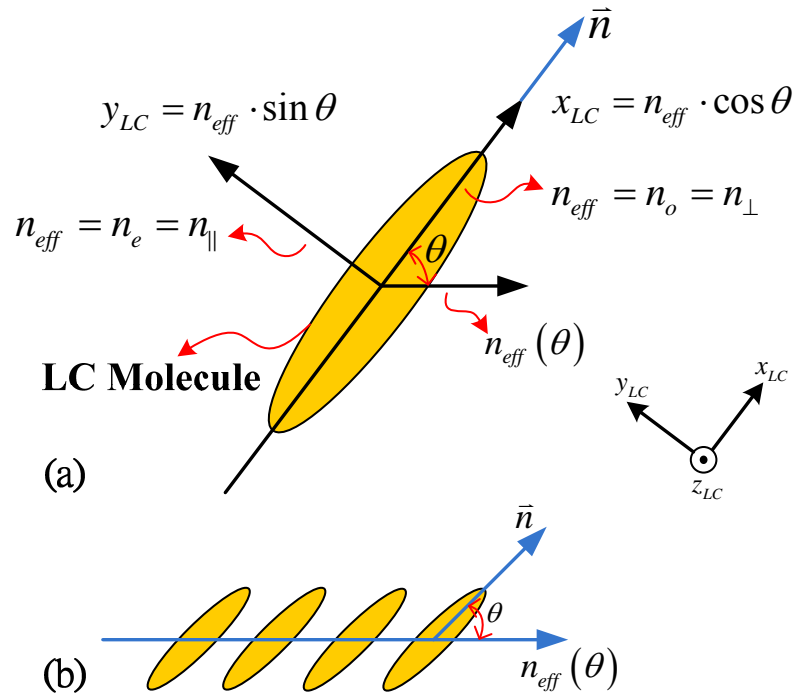
Fig. 24 (a) The ellipsoid of revolution representing $n_{eff}(\theta)$; (b) propagation of the

extraordinary beam obliquely through LC molecules.
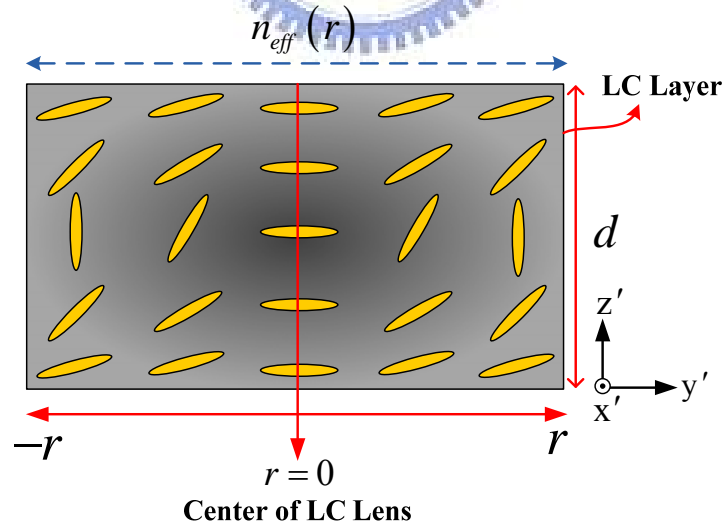
Fig. 25 The effective index distribution of refraction $n_{eff}(r)$ is illustrated that one is a

function of the radius r.
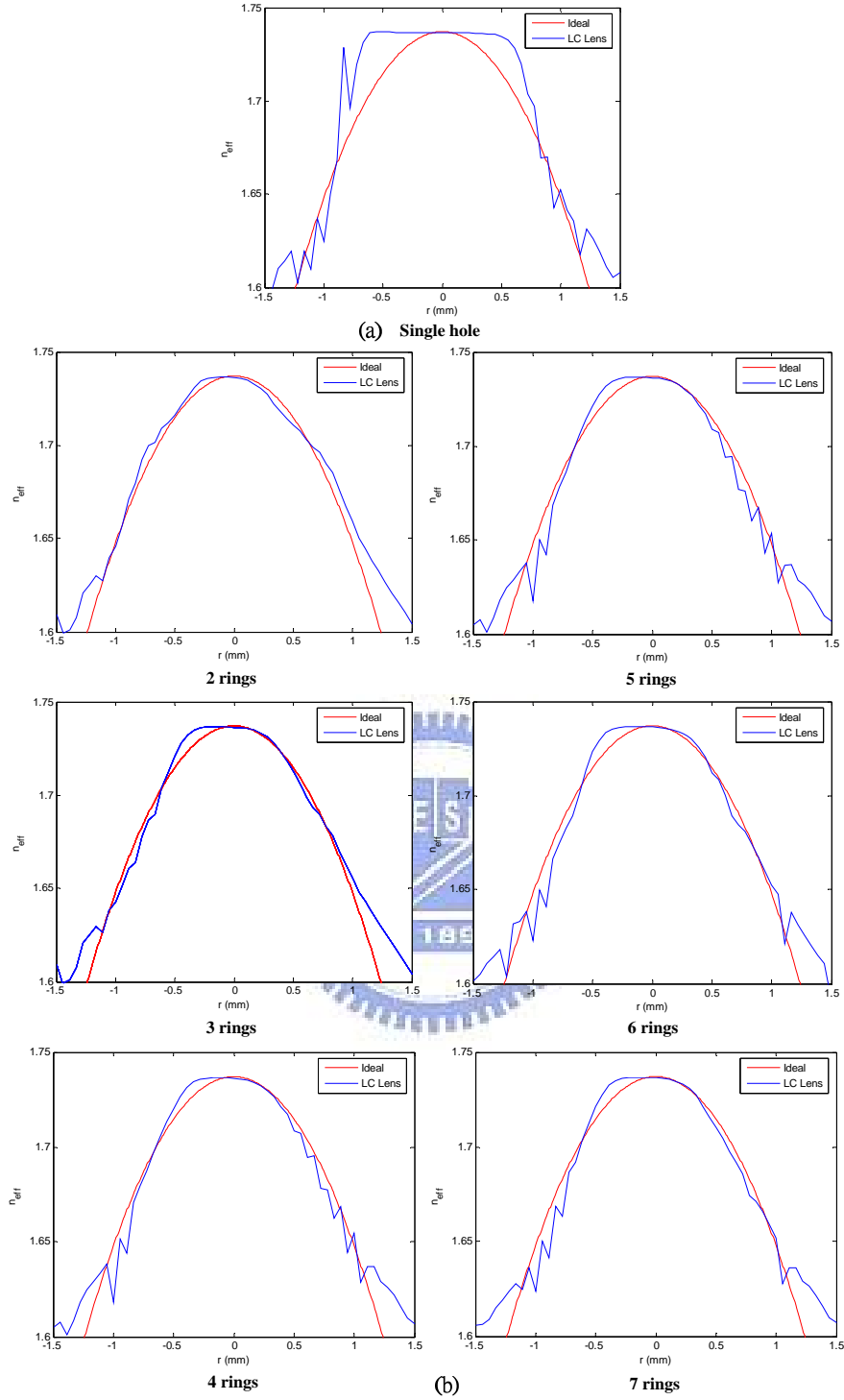
Fig. 26 Compared with the index distribution of GRIN lens which the focal length is also

112mm (Ideal case) and the effective index distribution of refractive $n_{eff}(r)$ of LC

lens (the wave length of light λ=633nm): (a) the LC lens with only single-hole

electrode; (b) the LC lens with the number of ring electrodes from two to seven rings

in different layers.
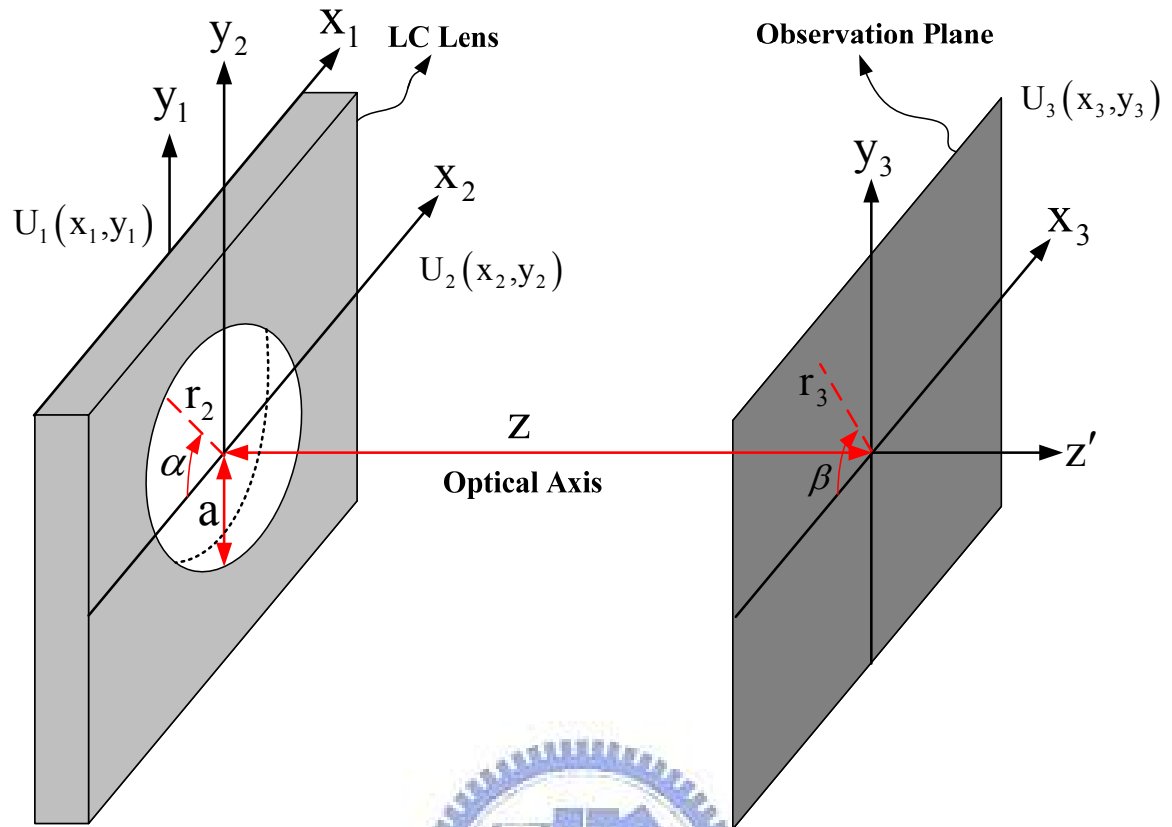
Fig. 27 The circular aperture of LC lens geometry illustrates the relative parameters for the calculation of PSF.

(a)

(b)
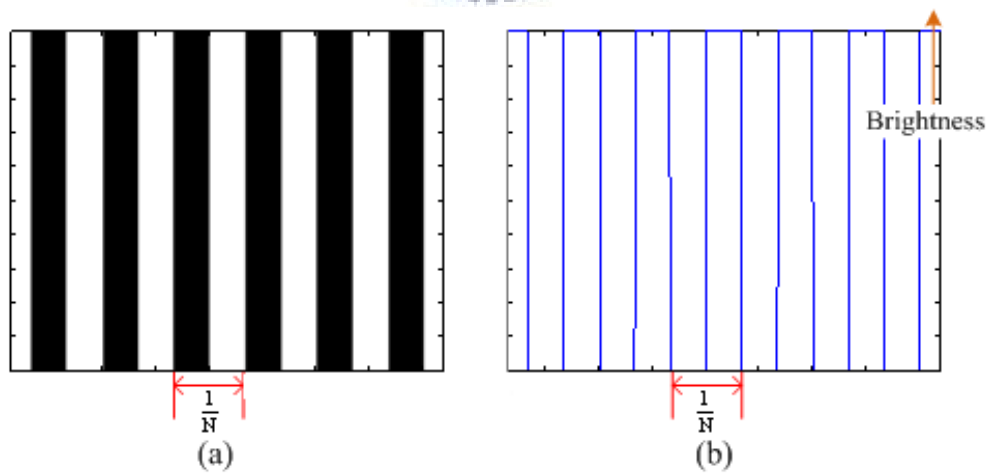
Fig. 28 The imagery of a bar target: (a) a typical bar target used in testing optical systems consists of alternating brightness and dark bars. If the pattern has a frequency of N lines per millimeter, then it has a period of $1/N$ millimeters, as indicated; (b) a plot of the brightness of (a) is a square wave.
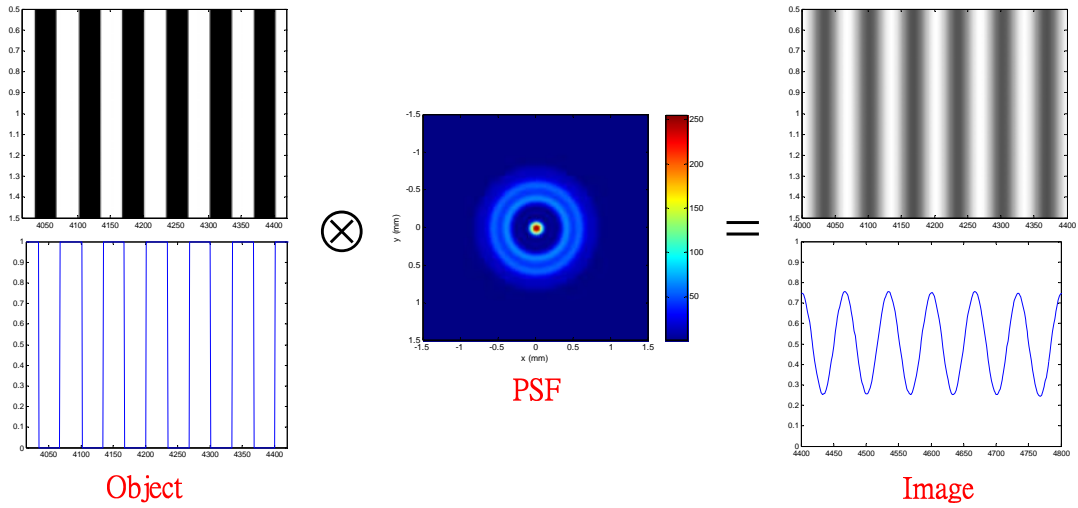
Fig. 29 The calculation of MTF by modulation is constructed by the operation of convolution, where $\otimes$ is a convolution operator.
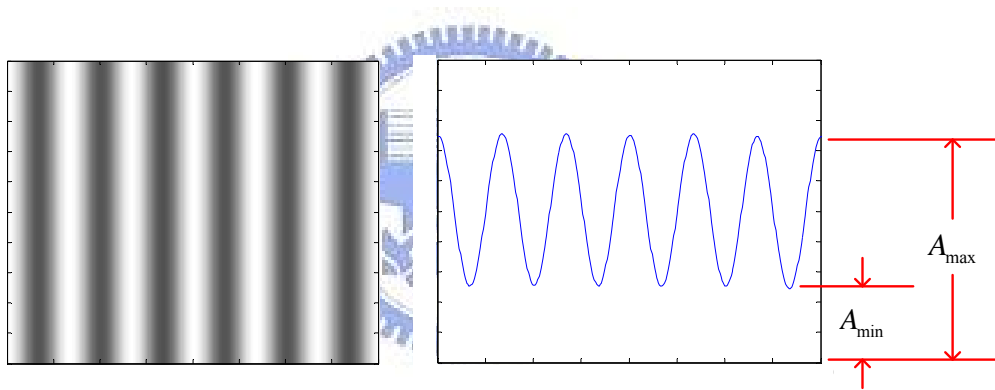
Fig. 30 As the test pattern is made finer, the contrast between the brightness and dark areas of the image is reduced.
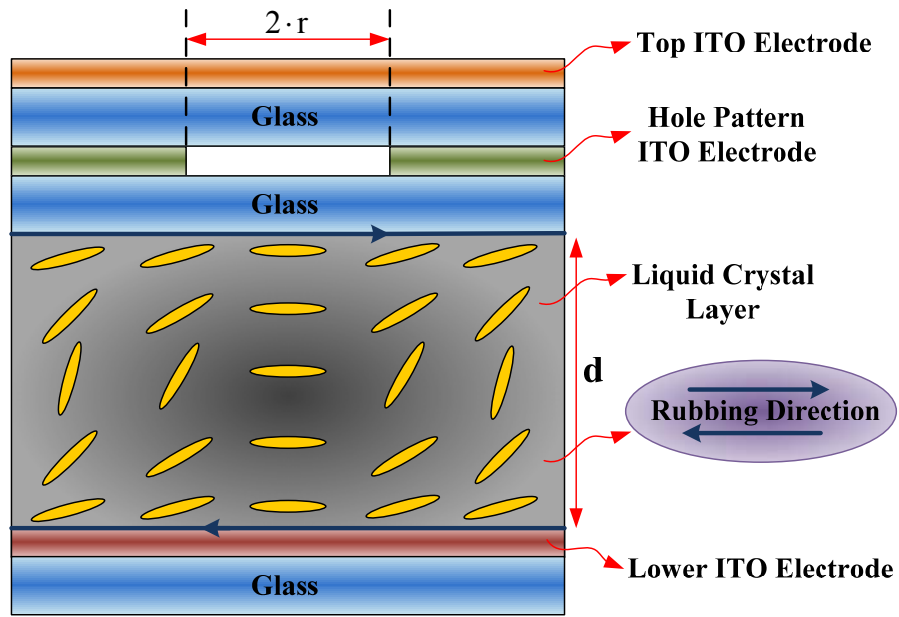
Fig. 31 The LC lens with the hole-type electrode that the diameter of effective aperture and the length of square shape are 3mm and 20mm respectively in our laboratory.

10V_{rms} 25V_{rms} 40V_{rms}

15V_{rms} 30V_{rms} 45V_{rms}

20V_{rms} 35V_{rms} 50V_{rms}
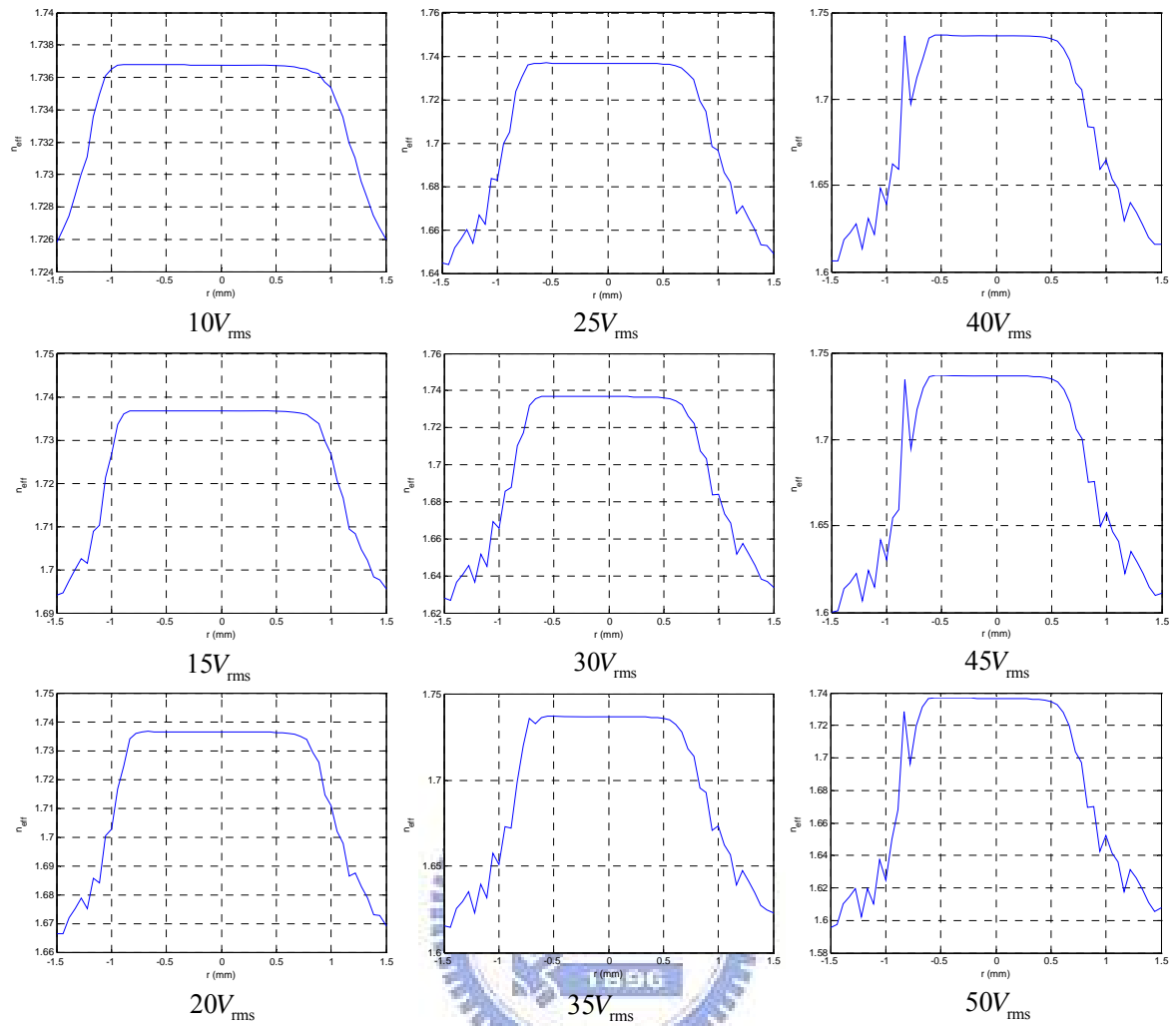
Fig. 32   By given the applied voltage form $10V_{\mathrm{rms}}$ to $50V_{\mathrm{rms}}$ in $5V_{\mathrm{rms}}$ steps for the LC lens with the hole-type electrode in our laboratory, their calculating results of effective index distribution of refractive $n_{eff}(r)$ are shown respectively (the wave length of light λ=633nm).
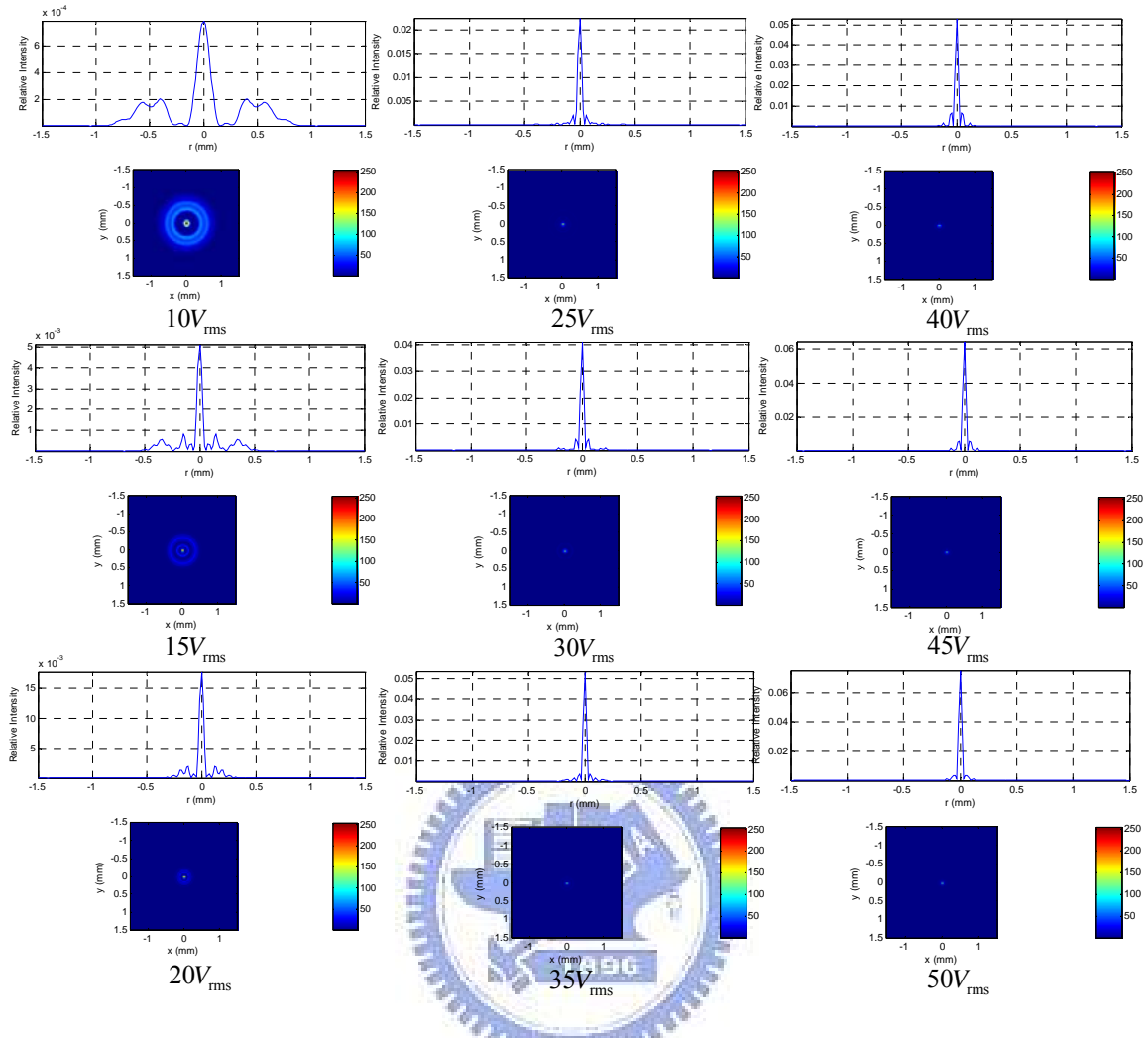
Fig. 33 By given the applied voltage form $10V_{rms}$ to $50V_{rms}$ in $5V_{rms}$ steps for the LC lens

with the hole-type electrode in our laboratory, their calculating results of irradiance

distribution as the PSF are shown respectively (the wave length of light λ=633nm).
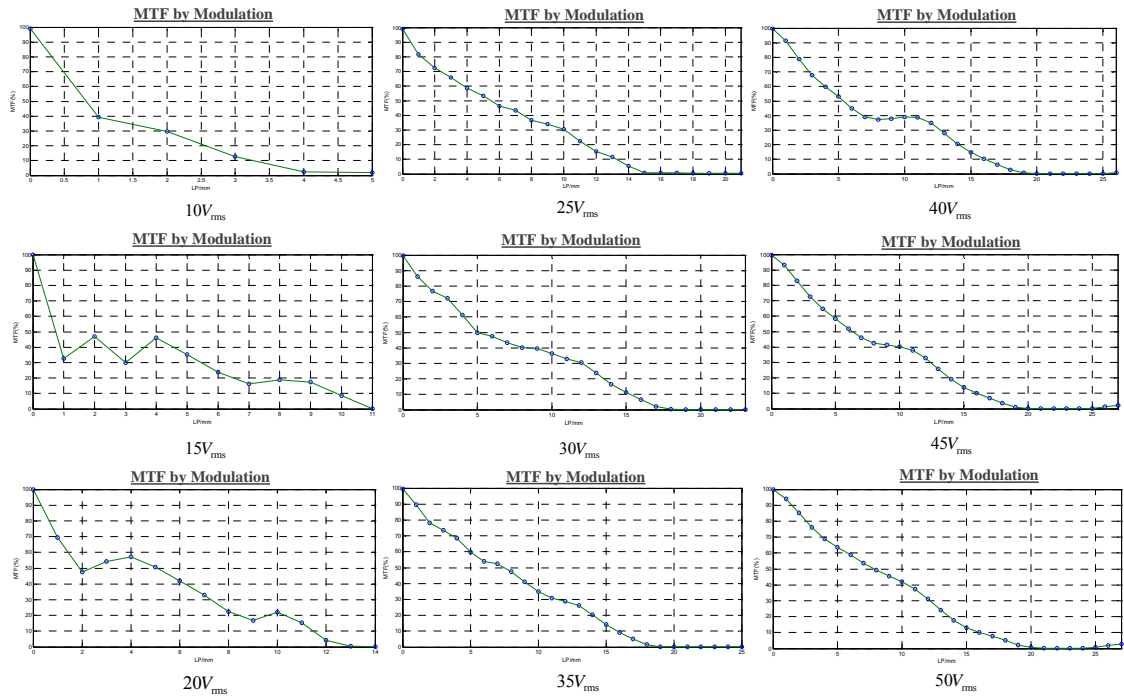
Fig. 34 By given the applied voltage form $10V_{rms}$ to $50V_{rms}$ in $5V_{rms}$ steps for the LC lens with the hole-type electrode in our laboratory, their calculating results of MTF are shown respectively (the wave length of light λ=633nm).
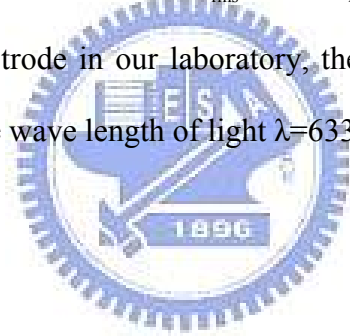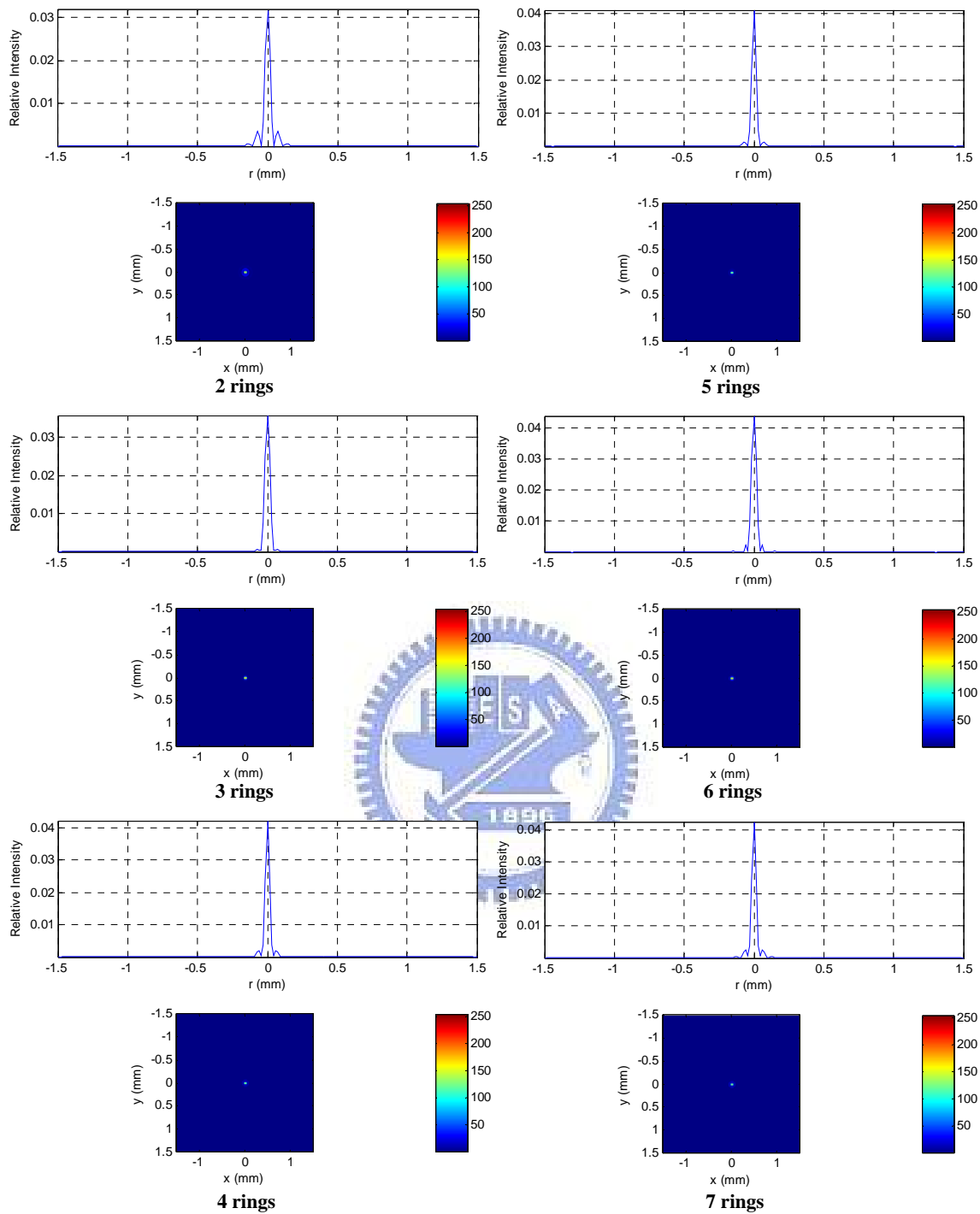
Fig. 35 The calculating results of irradiance distribution as the PSF of the LC lens with the number of ring electrodes from two to seven rings in different layers where its observation plane has the highest peak of relative intensity are shown respectively (the wave length of light λ=633nm).
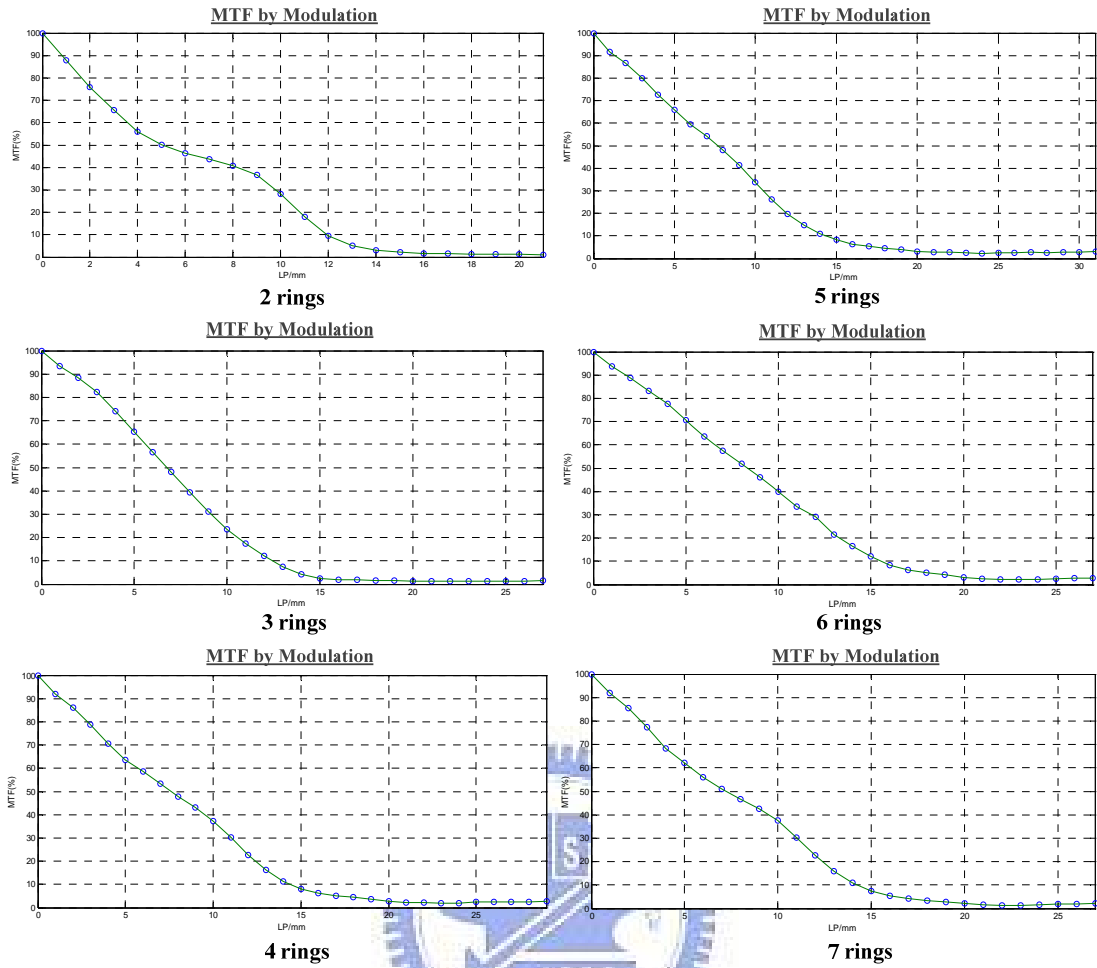
Fig. 36 The calculating results of MTF for the LC lens with the number of ring electrodes from two to seven rings in different layers where its observation plane has the highest peak of relative intensity are shown respectively (the wave length of light λ=633nm).

The MTF by Modulation of LC Lens With Multi-ring Electrodes in Different Layer
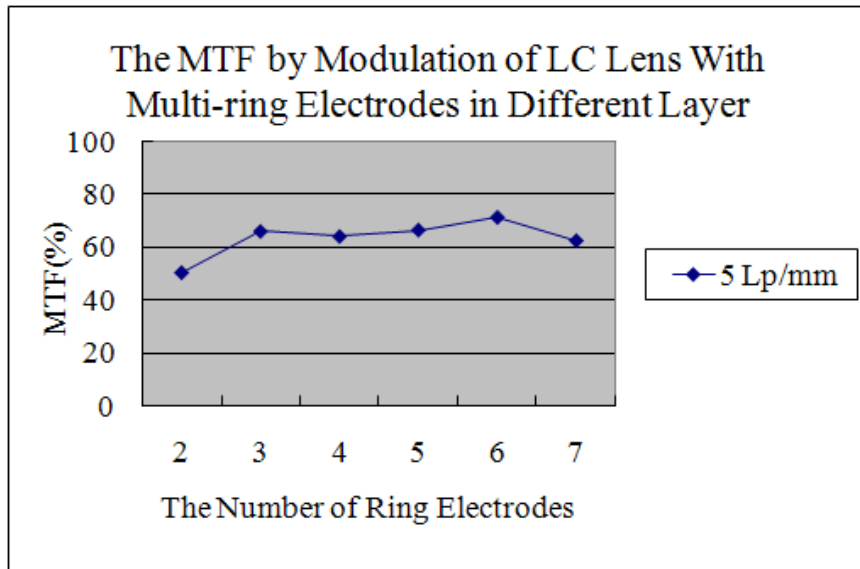
Fig. 37 As the calculating results of MTF where its observation plane has the highest peak of relative intensity, the MTF corresponding to 5 Lp/mm from the LC lens with the number of ring electrodes from two to seven rings in different layers are illustrated (the wave length of light λ=633nm).

The MTF by Modulation of LC Lens With Multi-ring Electrodes in Different Layer
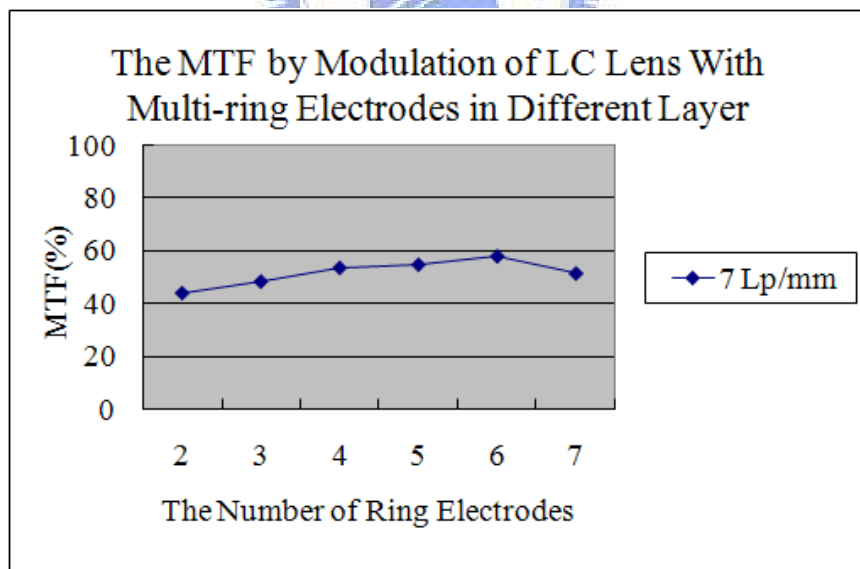
Fig. 38 As the calculating results of MTF where its observation plane has the highest peak of relative intensity, the MTF corresponding to 7 Lp/mm from the LC lens with the number of ring electrodes from two to seven rings in different layers are illustrated (the wave length of light λ=633nm).

Tables

Table 1: The specifications of two general lenses for cameras in cell phones. [28]

Cell phone lens No.	Cell phone lens 1	Cell phone lens 2
Pixel	1.3M	2.0M
Composition	3 Plastic	3 Plastic
Sensor	1/5"	1/4" CMOS
FNO	F2.8	F3.2
EFL	2.77mm(Paraxial)	3.36mm(Paraxial)

Table 2: The lens-group-moving distance is calculated along the optical axis based on the theory of traditional AF system.

Cell phone lens No.	Cell phone lens 1			Cell phone lens 2		
The distance of shot (d_{camera})	100	150	600	100	150	600
The lens-group-moving distance (X')	0.08	0.053	0.013	0.12	0.079	0.019
The unit: mm						

Table 3: The specifications of general optical glass lens with diameter 3mm.

Diameter	EFL	Center Thickness
The General Optical Plano-convex Lens		
3	3	2.3
3	4.5	2
3	6	1.8
3	9	1.6
The General Optical Plano-concave Lens		
3	-6	1.17
3	-9	1.11
3	-18	1.56
The unit: mm		

Table 4: The zooming system includes a positive LC lens for cameras in cell phones with the function of zooming.

Form f_{EFL}^{1x} to f_{EFL}^{2x}	f_{Lens}	f_1	From $f_{LC\ Lens}^{1x}$ to $f_{LC\ Lens}^{2x}$
Zooming			
300→150	-6	6.037	229.602→130
400→200	-6	6.098	193.5→130
500→250	-6	6.136	175.811→130
600→300	-6	6.161	166→130
600→300→200	-6	6.098	229.602→166→130
The unit: mm			

Table 5: With the same specifications of Form f_{EFL}^{1x} to f_{EFL}^{2x} and f_1 in Table 4, the movement saved by LC lens and the separation $d_{separation}$ for traditional zooming system are calculated.

Form f_{EFL}^{1x} to f_{EFL}^{2x}	f_2	f_1	$d_{separation}$	The Movement Saved by LC Lens
Zooming				
300→150	-6.161	6.037	0.124	3.08
400→200	-6.192	6.098	0.0948	3.11
500→250	-6.212	6.136	0.0765	3.12
600→300	-6.225	6.161	0.0638	3.11
600→200	-6.225	6.161	0.128	4.16
The unit: mm				

Table 6: The zooming system includes a negative LC lens for cameras in cell phones with the function of zooming.

Form f_{EFL}^{1x} to f_{EFL}^{2x}	f_{Lens}	f_2	From $f_{LC\ Lens}^{1x}$ to $f_{LC\ Lens}^{2x}$
Zooming			
600→300	5.735	-6.061	-130→-165.396
500→250	5.735	-6.073	-130→-175.272
400→200	5.735	-6.091	-130→-192.611
300→150	5.735	-6.122	-130→-229.478
200→100	5.735	-6.186	-130→-367.166
600→300→200	5.735	-6.061	-130→-165.396.5→-227.966
The unit: mm			

Table 7: With the same specifications of Form f_{EFL}^{1x} to f_{EFL}^{2x} and f_2 in Table 6, the movement saved by LC lens and the separation $d_{separation}$ for traditional zooming system are calculated.

Form f_{EFL}^{1x} to f_{EFL}^{2x}	f_1	f_2	$d_{separation}$	The Movement Saved by LC Lens
Zooming				
600→300	6	-6.061	0.0602	3.01
500→250	6	-6.073	0.0728	3.03
400→200	6	-6.091	0.0917	3.06
300→150	6	-6.122	0.123	3.07
200→100	6	-6.186	0.185	3.08
600→200	6	-6.061	0.121	4.03
The unit: mm				

Table 8: The relative parameters for the design of the LC lens with multi-ring electrodes in different layers and the specifications of LC are shown.

Items	Specifications
The Wave Length of Light	$\lambda=633$nm
The Thickness of Isolation Layer	1µm
The Thickness of ITO Electrodes	0.5µm
The Thickness of Glasses	550µm
The Thickness of LC Layer	50µm
The Dielectric Constant of Glass	$\varepsilon_{glass}=6.9$
The Specifications of LC	$K_{11}=11.1$ pN
	$K_{22}=5.9$ pN
	$K_{33}=17.1$ pN
	$\varepsilon_{\parallel}=19.28$
	$\varepsilon_{\perp}=5.21$
	$n_e=1.7371$
	$n_o=1.5183$

Table 9: The numerical values of slope dV/dr form the calculating result in Fig. 18 and its corresponding position of radius are listed to be the reference for the design of the LC lens with multi-ring electrodes.

The No. of position	The position of radius (±mm)	The width of electrode (μm)	The range of slope (dV/dr)	The difference in range of slope ($\Delta(dV/dr)$)
1.	10~1.5	8500	Non	Non
2.	1.5~1.489	11	3.748~3.464	0.284
3.	1.489~1.478	11	3.464~3.21	0.254
4.	1.478~1.467	11	3.21~2.981	0.229
5.	1.467~1.456	11	2.981~2.775	0.206
6.	1.456~1.445	11	2.775~2.589	0.186
7.	1.445~1.433	12	2.589~2.419	0.17
8.	1.433~1.421	12	2.419~2.265	0.154
9.	1.421~1.409	12	2.265~2.125	0.14
10.	1.409~1.396	13	2.125~1.996	0.129
11.	1.396~1.383	13	1.996~1.879	0.117
12.	1.383~1.371	12	1.879~1.771	0.108
13.	1.371~1.357	14	1.771~1.672	0.099

14.	1.357~1.344	13	1.672~1.58	0.092
15.	1.344~1.33	14	1.58~1.496	0.084
16.	1.33~1.316	14	1.496~1.418	0.078
17.	1.316~1.302	14	1.418~1.347	0.071
18.	1.302~1.288	14	1.347~1.28	0.067
19.	1.288~1.273	15	1.28~1.218	0.062
20.	1.273~1.258	15	1.218~1.161	0.057
21.	1.258~1.243	15	1.161~1.108	0.053
22.	1.243~1.228	15	1.108~1.059	0.049
23.	1.228~1.212	16	1.059~1.014	0.045
24.	1.212~1.196	16	1.014~0.9712	0.0428
25.	1.196~1.18	16	0.9712~0.9317	0.0395
26.	1.18~1.163	17	0.9317~0.8951	0.0366
27.	1.163~1.147	16	0.8951~0.8611	0.034
28.	1.147~1.13	17	0.8611~0.8296	0.0315
29.	1.13~1.113	17	0.8296~0.8003	0.0293
30.	1.113~1.095	18	0.8003~0.7732	0.0271
31.	1.095~1.078	17	0.7732~0.7482	0.025
32.	1.078~1.06	18	0.7482~0.725	0.0232
33.	1.06~1.042	18	0.725~0.7038	0.0212
34.	1.042~1.024	18	0.7038~0.6842	0.0196
35.	1.024~1.005	19	0.6842~0.6663	0.0179
36.	1.005~0.9869	18.1	0.6663~0.6501	0.0162
37.	0.9869~0.9681	18.8	0.6501~0.6354	0.0147
38.	0.9681~0.9491	19	0.6354~0.6222	0.0132
39.	0.9491~0.9299	19.2	0.6222~0.6105	0.0117
40.	0.9299~0.9106	19.3	0.6105~0.6002	0.0103
41.	0.9106~0.891	19.6	0.6002~0.5913	0.0089
42.	0.891~0.8713	19.7	0.5913~0.5838	0.0075
43.	0.8713~0.8515	19.8	0.5838~0.5776	0.0062
44.	0.8515~0.8315	20	0.5776~0.5728	0.0048
45.	0.8315~0.8114	20.1	0.5728~0.5693	0.0035
46.	0.8114~0.7911	20.3	0.5693~0.5672	0.0021
47.	0.7911~0.7708	20.3	0.5672~0.5665	0.0007
48.	0.7708~0.7503	20.5	0.5665~0.567	0.0005
49.	0.7503~0.7297	20.6	0.567~0.569	0.002
50.	0.7297~0.709	20.7	0.569~0.5723	0.0033

51.	0.709~0.6882	20.8	0.572~0.5769	0.0049
52.	0.6882~0.6673	20.9	0.5769~0.583	0.0061
53.	0.6673~0.6463	21	0.583~0.5904	0.0074
54.	0.6463~0.6253	21	0.5904~0.5992	0.0088
55.	0.6253~0.6042	21.1	0.5992~0.6094	0.0102
56.	0.6042~0.583	21.2	0.6094~0.6211	0.0117
57.	0.583~0.5618	21.2	0.6211~0.6341	0.013
58.	0.5618~0.5406	21.2	0.6341~0.6485	0.0144
59.	0.5406~0.5193	21.3	0.6485~0.6642	0.0157
60.	0.5193~0.498	21.3	0.6642~0.6813	0.0171
61.	0.498~0.4766	21.4	0.6813~0.6996	0.0183
62.	0.4766~0.4553	21.3	0.6996~0.7192	0.0196
63.	0.4553~0.4338	21.5	0.7192~0.7399	0.0207
64.	0.4338~0.4124	21.4	0.7399~0.7615	0.0216
65.	0.4124~0.391	21.4	0.7615~0.7841	0.0226
66.	0.391~0.3695	21.5	0.7841~0.8071	0.023
67.	0.3695~0.3479	21.6	0.8071~0.8303	0.0232
68.	0.3479~0.3263	21.6	0.8303~0.8527	0.0224
69.	0.3263~0.3046	21.7	0.8527~0.8724	0.0197
70.	0.3046~0.2827	21.9	0.8724~0.8844	0.012
71.	0.2827~0.2604	22.3	0.8844~0.8695	0.0149
72.	0.2604~0.237	23.4	0.8695~0.5679	0.3016
73.	0.237~0.2	37	0.5679~0	0.5679
74.	0.2~0	200	Non	Non

Table 10: According to the redistributions by the slope range considered, the numerical values of the position of radius and the width of electrode in Table 9 are separated into 12 groups.

The group of regularity	The range of No.	The position of radius (±mm)	The width of electrode (μm)	The slope range considered	The difference in varied range of slope
(1)	1	10~1.5	8500	Non	Non
(2)	2~3	1.5~1.478	22	0.25~0.3	0.05
(3)	4~5	1.478~1.456	22	0.2~0.25	0.05
(4)	6~8	1.456~1.421	35	0.15~0.2	0.05
(5)	9~12	1.421~1.371	50	0.1~0.15	0.05
(6)	13~21	1.371~1.243	128	0~0.05	0.05
(7)	22~40	1.243~0.9106	332.4	0.01~0.05	0.04
(8)	41~54	0.9106~0.6253	285.3	0~0.01	0.01
(9)	55~62	0.6253~0.4553	170	0.01~0.02	0.01
(10)	63~68	0.4553~0.3263	129	0.02~0.03	0.01
(11)	69~73	0.3263~0.2	126.3	0.01~0.02	0.01
(12)	Non	0.2~0	200	0	0

Table 11: The design for the widths of the LC lens with two-ring electrodes is shown.

The electrodes of the LC lens	The range of group with regularity	The position of radius (±mm)	The width of electrode (μm)
The hole-type	(1)	10~1.5	8500
The second ring	(2)~(11)	1.5~0.2	1300
The first ring	(12)	0.2~0	200

Table 12: The design for the widths of the LC lens with three-ring electrodes is shown.

The electrodes of the LC lens	The range of group with regularity	The position of radius (±mm)	The width of electrode (μm)
The hole-type	(1)	10~1.5	8500
The third ring	(2)~(7)	1.5~0.9106	589.4
The second ring	(8)~(11)	0.9106~0.2	710.6
The first ring	(12)	0.2~0	200
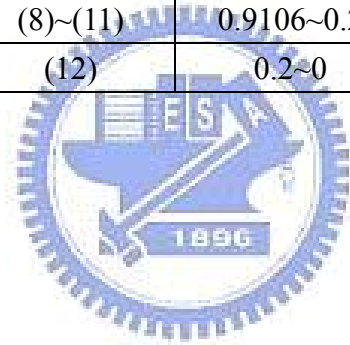
Table 13: The design for the widths of the LC lens with four-ring electrodes is shown.

The electrodes of the LC lens	The range of group with regularity	The position of radius (±mm)	The width of electrode (μm)
The hole-type	(1)	10~1.5	8500
The fourth ring	(2)~(5)	1.5~1.371	129
The third ring	(6)~(7)	1.371~0.9106	460.4
The second ring	(8)~(11)	0.9106~0.2	710.6
The first ring	(12)	0.2~0	200

Table 14: The design for the widths of the LC lens with five-ring electrodes is shown.

The electrodes of the LC lens	The range of group with regularity	The position of radius (±mm)	The width of electrode (μm)
The hole-type	(1)	10~1.5	8500
The fifth ring	(2)~(4)	1.5~1.421	79
The fourth ring	(5)~(6)	1.421~1.243	178
The third ring	(7)	1.243~0.9106	332.4
The second ring	(8)~(11)	0.9106~0.2	710.6
The first ring	(12)	0.2~0	200

Table 15: The design for the widths of the LC lens with six-ring electrodes is shown.

The electrodes of the LC lens	The range of group with regularity	The position of radius (±mm)	The width of electrode (μm)
The hole-type	(1)	10~1.5	8500
The sixth ring	(2)~(4)	1.5~1.421	79
The fifth ring	(5)~(6)	1.421~1.243	178
The fourth ring	(7)	1.243~0.9106	332.4
The third ring	(8)~(9)	0.9106~0.4553	455.3
The second ring	(10)~(11)	0.4553~0.2	255.3
The first ring	(12)	0.2~0	200

Table 16: The design for the widths of the LC lens with seven-ring electrodes is shown.

The electrodes of the LC lens	The range of group with regularity	The position of radius (±mm)	The width of electrode (μm)
The hole-type	(1)	10~1.5	8500
The seventh ring	(2)~(3)	1.5~1.456	44
The sixth ring	(4)~(5)	1.456~1.371	85
The fifth ring	(6)	1.371~1.243	128
The fourth ring	(7)	1.243~0.9106	332.4
The third ring	(8)~(9)	0.9106~0.4553	455.3
The second ring	(10)~(11)	0.4553~0.2	255.3
The first ring	(12)	0.2~0	200

Table 17: The design for the applied voltage of the LC lens with two-ring electrodes in different layers is shown.

The electrodes of the LC lens	The position of radius (±mm)	The range of applied voltage $V_{Single\text{-}layer}$ (V_{rms})	The range of applied voltage $V_{multi\text{-}layer}$ (V_{rms})
The hole-type	10~1.5	50	50
The second ring	1.5~0.2	2.216~0.9553	26.66~11.49
The first ring	0.2~0	0	0

Table 18: The design for the applied voltage of the LC lens with three-ring electrodes in different layers is shown.

The electrodes of the LC lens	The position of radius (±mm)	The range of applied voltage $V_{Single\text{-}layer}$ (V_{rms})	The range of applied voltage $V_{multi\text{-}layer}$ (V_{rms})
The hole-type	10~1.5	50	50
The third ring	1.5~0.9106	2.216~1.428	26.66~17.18
The second ring	0.9106~0.2	1.428~0.9553	17.22~11.52
The first ring	0.2~0	0	0

Table 19: The design for the applied voltage of the LC lens with four-ring electrodes in different layers is shown.

The electrodes of the LC lens	The position of radius (±mm)	The range of applied voltage $V_{Single\text{-}layer}$ (V_{rms})	The range of applied voltage $V_{multi\text{-}layer}$ (V_{rms})
The hole-type	10~1.5	50	50
The fourth ring	1.5~1.371	2.216~1.875	26.66~22.56
The third ring	1.371~0.9106	1.875~1.428	22.61~17.22
The second ring	0.9106~0.2	1.428~0.9553	17.26~11.55
The first ring	0.2~0	0	0

Table 20: The design for the applied voltage of the LC lens with five-ring electrodes in different layers is shown.

The electrodes of the LC lens	The position of radius (±mm)	The range of applied voltage $V_{Single\text{-}layer}$ (V_{rms})	The range of applied voltage $V_{multi\text{-}layer}$ (V_{rms})
The hole-type	10~1.5	50	50
The fifth ring	1.5~1.421	2.216~1.978	26.66~23.8
The fourth ring	1.421~1.243	1.978~1.692	23.85~20.41
The third ring	1.243~0.9106	1.692~1.428	20.46~17.26
The second ring	0.9106~0.2	1.428~0.9553	17.31~11.58
The first ring	0.2~0	0	0

Table 21: The design for the applied voltage of the LC lens with six-ring electrodes in different layers is shown.

The electrodes of the LC lens	The position of radius (±mm)	The range of applied voltage $V_{Single-layer}$ (V_{rms})	The range of applied voltage $V_{multi-layer}$ (V_{rms})
The hole-type	10~1.5	50	50
The sixth ring	1.5~1.421	2.216~1.978	26.66~23.8
The fifth ring	1.421~1.243	1.978~1.692	23.85~20.41
The fourth ring	1.243~0.9106	1.692~1.428	20.46~17.26
The third ring	0.9106~0.4553	1.428~1.154	17.31~13.95
The second ring	0.4553~0.2	1.154~0.9553	14.02~11.61
The first ring	0.2~0	0	0

Table 22: The design for the applied voltage of the LC lens with seven-ring electrodes in different layers is shown.

The electrodes of the LC lens	The position of radius (±mm)	The range of applied voltage $V_{Single-layer}$ (V_{rms})	The range of applied voltage $V_{multi-layer}$ (V_{rms})
The hole-type	10~1.5	50	50
The seventh ring	1.5~1.456	2.216~2.069	26.66~24.89
The sixth ring	1.456~1.371	2.069~1.875	24.95~22.61
The fifth ring	1.371~1.243	1.875~1.692	22.67~20.46
The fourth ring	1.243~0.9106	1.692~1.428	20.51~17.31
The third ring	0.9106~0.4553	1.428~1.154	17.35~14.02
The second ring	0.4553~0.2	1.154~0.9553	14.06~11.64
The first ring	0.2~0	0	0

Table 23: The width of each ring electrode and its applied voltage $V_{multi\text{-}layer}$ of the LC lens with two-ring electrodes in different layers for simulation are reorganized and determined.

The electrodes of the LC lens	The position of radius (±mm)	The width of electrode (μm)	The applied voltage $V_{multi\text{-}layer}$ (V_{rms})
The hole-type	10~1.5	8500	50
The second ring	1.5~0.2	1300	14.2
The first ring	0.2~0	200	0

Table 24: The width of each ring electrode and its applied voltage $V_{multi\text{-}layer}$ of the LC lens with three-ring electrodes in different layers for simulation are reorganized and determined.

The electrodes of the LC lens	The position of radius (±mm)	The width of electrode (μm)	The applied voltage $V_{multi\text{-}layer}$ (V_{rms})
The hole-type	10~1.5	8500	50
The third ring	1.5~0.9106	589.4	17.18
The second ring	0.9106~0.2	710.6	11.52
The first ring	0.2~0	200	0

Table 25: The width of each ring electrode and its applied voltage $V_{multi\text{-}layer}$ of the LC lens with four-ring electrodes in different layers for simulation are reorganized and determined.

The electrodes of the LC lens	The position of radius (±mm)	The width of electrode (μm)	The applied voltage $V_{multi\text{-}layer}$ (V_{rms})
The hole-type	10~1.5	8500	50
The fourth ring	1.5~1.371	129	22.56
The third ring	1.371~0.9106	460.4	17.22
The second ring	0.9106~0.2	710.6	13
The first ring	0.2~0	200	0

Table26: The width of each ring electrode and its applied voltage $V_{multi\text{-}layer}$ of the LC lens with five-ring electrodes in different layers for simulation are reorganized and determined.

The electrodes of the LC lens	The position of radius (±mm)	The width of electrode (μm)	The applied voltage $V_{multi\text{-}layer}$ (V_{rms})
The hole-type	10~1.5	8500	50
The fifth ring	1.5~1.421	79	23.8
The fourth ring	1.421~1.243	178	20.41
The third ring	1.243~0.9106	332.4	17.26
The second ring	0.9106~0.2	710.6	13
The first ring	0.2~0	200	0

Table 27: The width of each ring electrode and its applied voltage $V_{multi-layer}$ of the LC lens with six-ring electrodes in different layers for simulation are reorganized and determined.

The electrodes of the LC lens	The position of radius (±mm)	The width of electrode (μm)	The applied voltage $V_{multi-layer}$ (V_{rms})
The hole-type	10~1.5	8500	50
The sixth ring	1.5~1.421	79	23.8
The fifth ring	1.421~1.243	178	20.41
The fourth ring	1.243~0.9106	332.4	17.26
The third ring	0.9106~0.4553	455.3	11
The second ring	0.4553~0.2	255.3	10.5
The first ring	0.2~0	200	0

Table 28: The width of each ring electrode and its applied voltage $V_{multi-layer}$ of the LC lens with seven-ring electrodes in different layers for simulation are reorganized and determined.

The electrodes of the LC lens	The position of radius (±mm)	The width of electrode (μm)	The applied voltage $V_{multi-layer}$ (V_{rms})
The hole-type	10~1.5	8500	50
The seventh ring	1.5~1.456	44	24.89
The sixth ring	1.456~1.371	85	22.61
The fifth ring	1.371~1.243	128	20.46
The fourth ring	1.243~0.9106	332.4	17.31
The third ring	0.9106~0.4553	455.3	13.5
The second ring	0.4553~0.2	255.3	11.64
The first ring	0.2~0	200	0

Table 29: The relative parameters for the design of the LC lens with the hole-type electrode and the specifications of LC in our laboratory are shown.

Items	Specifications
The Wave Length of Light	λ=633nm
The Thickness of ITO Electrodes	1μm
The Thickness of Glasses	550μm
The Thickness of LC Layer	50μm
The Dielectric Constant of Glass	$\varepsilon_{glass} = 6.9$
The Specifications of LC	$K_{11} = 11.1$ pN
	$K_{22} = 5.9$ pN
	$K_{33} = 17.1$ pN
	$\varepsilon_{\parallel} = 19.28$
	$\varepsilon_{\perp} = 5.21$
	$n_e = 1.7371$
	$n_o = 1.5183$

自傳

姓名 : 施凱騰

籍貫 : 台 灣 省 台北市

出生日期 : 民 國 72 年 11 月 08 日

學歷 : 民 國 85 年 台 北 市 西 門 國 小 畢

　　　 民 國 88 年 台 北 縣 東 海 中 學 畢

　　　 民 國 91 年 台 北 縣 東 海 中 學 畢

　　　 民 國 95 年 國 立 嘉 義 大 學 生 物 機 電 工 程 系 畢

　　　 民 國 97 年 國 立 交 通 大 學 電 機 與 控 制 工 程 研 究 所 甲 組 畢

E – Mail : kaiteng.ece95g@nctu.edu.tw

電 話 : 0911281484